The structure of AgamOBP5 in complex with the natural insect repellents Carvacrol and Thymol: Crystallographic, fluorescence and thermodynamic binding studies

Panagiota G.V. Liggri[1,2], Katerina E. Tsitsanou[1], Evgenia C.V. Stamati[1,2], Francesca Saitta[3], Christina E. Drakou[1§], Demetres D. Leonidas[2], Dimitrios Fessas[3] and Spyros E. Zographos*[,1]

[1]Institute of Chemical Biology, National Hellenic Research Foundation, 48 Vassileos Constantinou Avenue, 11635 Athens, Greece

[2]Department of Biochemistry and Biotechnology, University of Thessaly, Biopolis, 41500 Larissa, Greece

[3]Department of Food, Environmental and Nutritional Sciences, Università degli Studi di Milano, Via Celoria 2, 20133 Milano, Italy

Running Title: *The crystal structure of AgamOBP5 with Carvacrol and Thymol*

[§]current address: Department of Biochemistry and Biotechnology, University of Thessaly, Biopolis, 41500 Larissa, Greece

[*]to whom correspondence should be addressed at Institute of Biology, Medicinal Chemistry & Biotechnology, National Hellenic Research Foundation, 48 Vassileos Constantinou Avenue, 11635 Athens, Greece. Tel: +30-2107273850. E-mail: sez@eie.gr

Abstract

Among several proteins participating in the olfactory perception process of insects, Odorant Binding Proteins (OBPs) are today considered valid targets for the discovery of compounds that interfere with their host-detection behavior. The 3D structures of *Anopheles gambiae* mosquito AgamOBP1 in complex with the known synthetic repellents DEET and Icaridin have provided valuable information on the structural characteristics that govern their selective binding.

However, no structure of a plant-derived repellent bound to an OBP has been available until now. Herein, we present the novel three-dimensional crystal structures of AgamOBP5 in complex with two natural phenolic monoterpenoid repellents, Carvacrol and Thymol, and the MPD molecule.

Structural analysis revealed that both monoterpenoids occupy a binding site (Site-1) by adopting two alternative conformations. An additional Carvacrol was also bound to a secondary site (Site-2) near the central cavity entrance. A protein-ligand hydrogen-bond network supplemented by van der Waals interactions spans the entire binding cavity, bridging α4, α6, and α3 helices and stabilizing the overall structure.

Fluorescence competition and Differential Scanning Calorimetry experiments verified the presence of two binding sites and the stabilization effect on AgamOBP5. While Carvacrol and Thymol bind to Site-1 with equal affinity in the submicromolar range, they exhibit a significantly lower and distinct binding capacity for Site-2 with Kd's of ~7 μM and ~18 μM, respectively.

Finally, a comparison of AgamOBP5 complexes with the AgamOBP4-Indole structure revealed that variations of ligand-interacting aminoacids such as A109T, I72M, A112L, and A105T cause two structurally similar and homologous proteins to display different binding specificities.

Abbreviations: OBP, Odorant Binding Protein; AgamOBP, *Anopheles gambiae* odorant binding protein; 1-NPN, N-phenyl-1-naphthylamine; MPD, 2-Methyl-2,4-pentanediol

Keywords: Odorant binding protein, OBP, mosquito, Repellent, Carvacrol, Thymol

INTRODUCTION

Dangerous parasites and viruses are transmitted to humans through the bites of infected mosquitoes causing fatal diseases such as malaria, dengue fever, Zika, chikungunya, West Nile virus, and other vector-borne afflictions. In 2020, malaria caused an

estimated 241 million clinical cases and approximately 627.000 deaths globally, of which nearly 96% (602.000 deaths) were in the African region and 77% were of children aged under five [1]. Today, malaria prevention mainly relies on personal protection measures against mosquito bites, as no effective vaccines or prophylactic drugs are currently available [2]. Insect repellents are considered the most reliable means of human defense against mosquitoes and other blood-sucking arthropods [3, 4]. Although these agents provide excellent and long-term protection, they raise safety concerns regarding their potential mammalian toxicity and carcinogenicity [5-8], as well as the development of resistance in mosquitoes [2, 9-12].

Over the last decade, there has been an increased focus on natural plant-derived repellents as they are perceived by consumers as "purer", environmentally friendly, and safer than synthetic ones. Plants with repellent properties that have been used in traditional practices for centuries constitute a valuable source for the development of new natural products. Several plant-based compounds of different chemical classes including carvacrol, thymol, geraniol, citronellol, citronellal, cumin aldehyde, cuminic acid, benzyl benzoate, and methyl-, ethyl- and n-butyl-cinnamate have been found to exert a repellent effect on mosquitoes [13-16], thus representing promising alternatives to synthetic chemical agents. Although significant progress has been made towards understanding the chemical ecology of mosquitoes [17, 18], the molecular mechanism of the perception of repellents, whether of synthetic or natural origin, is still not well understood.

Anopheles gambiae is the primary vector in sub-Saharan Africa responsible for the transmission of the malaria parasite *Plasmodium falciparum*. Female mosquitoes rely mainly on olfactory cues to locate their human hosts in order to take a blood-meal from them. Therefore, novel strategies targeting the mosquito olfactory system are considered promising tools to control their host-seeking behavior. Insect Odorant Binding Proteins (OBPs) and Odorant Receptors (ORs) are essential components of the olfactory signal

transduction cascade, highly contributing to the sensitivity and selectivity of insect olfaction [19]. Lipophilic odorant molecules entering the aqueous sensillum lymph of mosquito antenna are captured by the OBPs in order to be solubilized and transported to the ORs, triggering a response. OBPs which are small soluble proteins secreted into the lymph in extremely high levels (up to 10 mM) [20], are considered today as valid targets for the identification of compounds that interfere with the olfactory system of insects. OBPs have been proposed to contribute to odor recognition as the first filter of selection as they are able to distinguish between chemically divergent odorants, with each one of these proteins recognizing a class of structurally related molecules [13, 21-27]. Several studies have reported their involvement in the detection of plant-derived volatile compounds [28-32], pheromones [33-37] as well as host and oviposition attractants [38-41].

Ten OBPs out of more than 69 encoded in the *Anopheles gambiae* genome [42] are likely to be involved in the human detection process as they are abundant in the antenna of female mosquitoes and their expression levels decrease after a blood meal. AgamOBP5 was ranked as No 1 in this subset of ten, exhibiting the highest mRNA levels in the antenna according to microarray analysis results [43]. Furthermore, a detailed gene expression study revealed that AgamOBP5 is significantly down-regulated in female mosquitoes three hours after a blood meal compared to the non-blood fed females, thus indicating its important role in host-seeking behavior [44].

AgamOBP5 shares a high degree of sequence identity with AgamOBP4 (62%) and *Drosophila melanogaster* LUSH protein (44%). Both AgamOBP5 and AgamOBP4 display a rhythmic expression with peaks around the day/night transitions, reaching maximum levels 3h before dusk and at the end of dusk/early night phase [45, 46]. Despite their common expression patterns, high protein sequence homology, and predicted structural similarity [47], these proteins probably recognize and bind odorants of different chemical structures. Specifically, fluorescence competitive binding assays have shown that the AgamOBP4

protein can tightly bind the acyclic monoterpene citronellal (IC50 = 1.23 μM, and Ki = 0.71 μM), whereas AgamOBP5 exhibits a low affinity for this volatile compound (IC50 = 182.91 μM, and Ki = 128.57 μM) [47].

The ongoing elucidation of OBPs' three-dimensional crystal structures in apo form or in complex with volatiles has greatly facilitated the *in silico* structure-based virtual screening and docking approaches for the identification of novel disruptors of the host-seeking behavior of insects [26, 48-54]. To date, the only available 3D structures of a mosquito OBP complexed with a repellent are those of AgamOBP1 with the known synthetic repellents DEET [55] and Icaridin [56], and the repelling component of the human sweat 6-methyl-5-hepten-2-one (6-MH) [57], which have provided valuable information on the structural characteristics that govern ligand-selective binding to the protein. However, no structure of any OBP with a plant-derived repellent molecule has yet been reported.

Here in, we present the novel three-dimensional crystal structure of AgamOBP5 at the high resolution of 1.35 Å. Structural comparison with its AgamOBP4 similar protein revealed structural differences that may play a role in odorant recognition. *In vitro* screening of plant-derived molecules through a fluorescence competition assay revealed that Carvacrol and Thymol bind to AgamOBP5 with enhanced affinity. Differential Scanning Calorimetry (DSC) experiments further verified the binding of these two phenolic monoterpenoids to the protein. Finally, a co-crystallization attempt of AgamOBP5 with either Carvacrol or Thymol led to the determination of their 3D complex structures at 1.3 Å resolution. The detailed structural analysis revealed that Carvacrol and Thymol occupy a site located at the bottom of a central cavity. Interestingly, for Carvacrol a second binding site close to the mouth opening was identified.

The determination of novel OBP and OBP-odorant/repellent complex structures will reveal the location of odorant/repellent-binding sites and the interactions that govern their complementary binding to the protein, further contributing to the understanding of their

perception mechanism. This detailed structural information on OBP targets is expected to greatly accelerate the discovery of new plant-based, more effective, safer, and eco-friendly mosquito control agents.

EXPERIMENTAL PROCEDURES

Bacterial Expression of AgamOBP5

AgamOBP5 cDNA (GenBank: AF437888; UNP: Q8T6K2) was PCR-amplified and subcloned into the NdeI and XhoI restriction sites of the pET22b(+) expression vector (Novagen). The pET22b(+)-AgamOBP5 plasmid was transformed into *Escherichia coli* Origami B(DE3) competent cells (Novagen). Protein expression was induced by 1mM IPTG (Isopropyl β-d-1-thiogalactopyranoside) at OD_{600} of 0.5–0.6 and allowed to proceed for 4h at 37°C. After centrifugation of the cell lysate at 15,000x*g* for 30 min at 4°C, the supernatant and pellet samples were subjected to 15% SDS-PAGE analysis. The protein was expressed at a high level in *E. coli*, mainly in the form of inclusion bodies (>80%).

Purification of Recombinant Protein from Inclusion Bodies

The protein was recovered from the inclusion bodies by the denaturation/refolding method of Boix [58], with minor modifications. Refolded protein was first applied to a Resource Q chromatographic column (GE Healthcare) equilibrated with 10 mM Tris–HCl, pH 8.0. AgamOBP5 (pI 8.53) eluted exclusively in the unbound fraction, while contaminant proteins were retained on the column. After overnight dialysis against 150 mM sodium acetate, pH 5.0, and clarification centrifugation (17,000 x g for 30 min at 4 °C) to remove precipitated proteins, the AgamOBP5 was recovered in the supernatant fraction.

In the final purification step, the protein fraction was subjected to Size-Exclusion Chromatography (SEC) on a Superdex75 16/73 column (GE Healthcare) equilibrated with 10

mM Tris-HCl, pH 8.0 and 200 mM NaCl. AgamOBP5 protein was obtained in a final yield of approximately 5 mg per liter of cell culture. In order to delipidate AgamOBP5, the purified protein at a concentration of 100 µM was treated with Lipidex-1000 resin (PerkinElmer Inc.), as described by Oldman et al. [59]. The delipidated protein was dialyzed against HPLC water, concentrated to 12 mg/mL, and used in the crystallization experiments. In the case of fluorescent binding assays and calorimetric experiments, the protein was buffer exchanged into 10-20 mM Tris-HCl (pH 8) containing 100 mM NaCl.

Crystallization and Data Collection

AgamOBP5 crystals were grown at 20°C by the sitting drop vapor diffusion method from a protein solution comprising 12 mg/ml AgamOBP5, 0.12M Monosaccharides (0.02 M each of D-Glucose, D-Mannose, D-Galactose, L-Fucose, D-Xylose and N-Acetyl-D-Glucosamine), 0.1 M Bicine/Trizma base pH 8.5, 12.5% (w/v) PEG 1000, 12.5% (w/v) PEG 3350 and 12.5% (v/v) MPD (2-Methyl-2,4-pentanediol). Co-crystals of AgamOBP5 with Carvacrol and Thymol were obtained in a precipitant solution containing 0.12M alcohols (0.02 M each of 1,6-Hexanediol, 1-Butanol, 1,2-Propanediol (racemic), 2-Propanol, 1,4-Butanediol and 1,3-Propanediol), 0.1 M MOPS/HEPES-Na pH 7.5, 12.5% (w/v) PEG 1000, 12.5% (w/v) PEG 3350, 12.5% (v/v) MPD, 2% (v/v) Methanol and 1mM Carvacrol or 1 mM Thymol, respectively. X-ray data were collected from single monoclinic crystals ($P2_1$) at 100K on I03 and I04-1 beamlines of the Diamond Light Source (Oxford, UK) to a maximum resolution of 1.3 to 1.35 Å.

Structure Determination

Diffraction data were integrated and scaled with the programs XDS and SCALA of the CCP4 suite [60]. The intensities were converted to amplitudes using TRUNCATE [61]. The initial phases of the AgamOBP5-MPD complex were determined by MOLREP [62] using the

AgamOBP4-indole structure (PDB id : 3Q8I) as a molecular replacement model. In the case of AgamOBP5-Carvacrol/Thymol complexes, the molecular replacement solution was obtained using the AgamOBP5-MPD structure as the search model. Several cycles of manual building were carried out by COOT. Maximum likelihood refinement (composed of positional minimization, and isotropic and anisotropic *B-factor* optimization) was performed using the program REFMAC5 [63] to improve model phases. Water molecules were added to unidentified F_o–F_c map peaks greater than 2.0σ using COOT and were manually inspected. Furthermore, a sodium ion and a PEG molecule were fitted into the electron density of AgamOBP5-MPD. Correspondingly, one sodium ion, an 1-butanol, an S-1,2-propanediol and an R-1,2-propanediol molecule were fitted into the AgamOBP5-Carvacrol, while two sodium ions, an S-1,2-propanediol and a PEG molecule were fitted into the AgamOBP5-Thymol model. After an additional cycle of refinement and manual building, the MPD and Thymol models, retrieved from the PDB, and the Carvacrol model, generated by PRODRG server [64], were fitted into the electron density and included in subsequent refinement cycles. Details of data processing and refinement statistics are summarized in **Table 1**.

The quality of the final structures was validated using the MolProbity [65] and PDB-REDO [66] servers. Structural superpositions were carried out with the LSQKAB program [60]. Volume of protein cavities, solvent accessible surface areas and protein mouths were analyzed by CASTp [67]. RMSD plots were generated with the MultiSeq module [68] of the VMD suite [69]. Plots of protein–ligand interactions were created with LIGPLOT [70]. The sequence alignment plot was created by ESPript v3.0 [71]. Figures of three dimensional structures and electron density were prepared with PyMOL [72]. The coordinates of the proteins have been deposited with the RCSB Protein Data Bank (http://www.rcsb.org/pdb) under accession codes **8BXU** (AgamOBP5-MPD), **8BXW** (AgamOBP5-Carvacrol) and **8BXV** (AgamOBP5-Thymol).

Table 1. Statistics of data collection, processing and refinement of the AgamOBP5 structures

AgamOBP5 Structure (PDB ID)	**MPD (8BXU)**	**Carvacrol (8BXW)**	**Thymol (8BXV)**
Data collection statistics			
MX Diamond Light Source	I03; λ=0.9762 Å	I04-1; λ=0.91587	I04-1; λ=0.91587
Space group $P2_1$, Cell dimensions; a,b,c (Å) α, β, γ (°)	33.94 35.51 55.06 90.00 100.49 90.00	34.36 36.71 54.66 90.00 101.77 90.00	34.24 36.57 54.96 90.00 100.38 90.00
Resolution (Å)	54.14 - 1.35	53.51 - 1.30	54.06 - 1.30
Outermost shell (Å)	1.42-1.35	1.37-1.30	1.37-1.30
Reflections measured	77102 (11354)	206235 (26351)	200594 (31980)
Unique reflections	27461 (3964)	32113 (4584)	31153 (4715)
Completeness %	96.5 (95.9)	97.5 (96.3)	94.3 (97.8)
Multiplicity	2.8 (2.9)	6.4 (5.7)	6.4 (6.8)
<I/σI>	12.7 (2.0)	23.5 (7.5)	22.5 (6.7)
Wilson Plot B-factor ($Å^2$)	17.42	15.3	16.86
Rsymm	0.036 (0.523)	0.036 (0.171)	0.037 (0.233)
Rmeas	0.045 (0.641)	0.040 (0.188)	0.040 (0.253)
$CC^{1/2}$	0.999 (0.749)	0.999 (0.985)	0.999 (0.980)
Refinement Statistics			
Final R_{cryst} / R_{free} %	16.57 / 19.41	17.18 / 20.09	18.51 / 22.02
No. of protein residues	123	123	123
No. of water molecules in final cycle	126	124	126
r.m.s. deviation in bond lengths (Å)	0.013	0.015	0.015
r.m.s. deviation in bond angles (°)	1.89	1.83	1.96
Average B factor ($Å^2$)			
Protein atoms	21.70	21.76	23.12
Water molecules	35.11	32.76	33.69
Ligand molecules	$34.14^{\text{All Ligands}}$, 24.06^{MPD1},	$32.20^{\text{All Ligands}}$, 45.30^{MPD}	$39.56^{\text{All Ligands,}}$ $57.05^{\text{MPD,}}$ 44.21^{PEU}

	35.12 MPD2, 35.64 MPD3, 44.02 PEU	21.93 Carvacrol Site 1 23.63 Carvacrol Site 2	29.03 Thymol Site 1
Ramachandran (u–w) plot.			
Residues in most favored regions (%)	99.17	100	100
Residues in allowed regions (%)	0.83	-	-

Data collection statistics for the highest-resolution shell are shown in parentheses.

Fluorescent measurements

The affinity of Carvacrol and Thymol for AgamOBP5 was evaluated indirectly by determining the displacement of the fluorescent probe 1-NPN by the ligand, as previously described [73]. In all experiments, the final assay mixture volume was 0.3 mL, and the assay buffer was 20 mM Tris-HCl, pH 8.0 and 100 mM NaCl. Fresh stock solutions of the fluorescent probe 1-NPN and of the tested compounds were prepared in methanol (100%) to be used in titration studies. The final methanol content was not greater than 2.83%. Fluorescence spectra were recorded on a Varioskan® Flash fluorimeter plate reader (Thermo Scientific) at 25 °C, using black 96-well plates (Greiner, Bio-One). The probe was excited at 337 nm and emission spectra were recorded from 360 nm to 500 nm. Maximal fluorescence emissions, in the presence of AgamOBP5, were observed between 402 nm and 410 nm, after subtraction of the background spectra (1-NPN and ligand in the buffer without protein). Fluorescence intensity means were obtained from triplicate measurements.

Ki determination of the selected ligands for AgamOBP5

The affinity of the fluorescent probe 1-NPN for AgamOBP5 was determined by titrating an AgamOBP5 solution (2 μM) with 1-NPN to final concentrations of 0 to 60 μM. The affinity

of the examined ligands for AgamOBP5 was calculated indirectly, by measuring their competition for 1-NPN binding. The AgamOBP5 was assayed at a final concentration of 2 μM and a constant concentration of 1-NPN (5μM). The probe was allowed to bind to AgamOBP5 before adding aliquots of ligand stock solution to achieve a final concentration range of 0 to 100 μM.

The equilibrium dissociation constants of 1-NPN (*K*d) and tested ligands (*K*i) were calculated using the non-linear regression data analysis program GraphPad Prism 8 (www.graphpad.com). The Kd of 1-NPN for AgamOBP5 was obtained by fitting the fluorescence intensity data to the saturation curve equation Y=Bmax*X/(Kd+X) for specific binding to one site (Supplemental **Figure S1**) and found to be 5.9 ± 0.4 μM. The *K*i's of Carvacrol and Thymol were determined by fitting the data to a competitive model for ligand binding to two sites using as HotNM the concentration of 1-NPN in the assays (5 μM) and as HotKdNM for both sites the calculated Kd of 1-NPN (5.9 μM), making the assumption that one molecule of 1-NPN occupies both binding sites.

Differential Scanning Calorimetry

Calorimetric measurements were carried out in solution with a protein concentration of about 0.2 mM in 10 mM Tris-HCl , pH 8.0, and 100 mM NaCl, with a TA Instruments Nano-DSC (6300) equipped with capillary cells at 0.5°C·min^{-1} scanning rate in the temperature range from 20°C to 110°C. When needed, ligands were added to protein from stock solutions in methanol up to the desired ligand-to-protein ratio ([L]/[P] = 15 or 7.5) just before launching the DSC measurement (methanol's final concentration in protein solutions was always equal to 2% v/v). The ligand-to-protein ratio of 15 was the maximum achievable one, compatible with our experimental conditions. Indeed, higher ligand concentrations would have led to ligand precipitation, whereas lower protein concentrations would not have been adequate for performing sufficiently good calorimetric measurements.

Data were analyzed through the software THESEUS [74] following procedures reported in previous studies [75, 76]. Briefly, the apparent molar heat capacity $C_P(T)$ of the sample was scaled taking as baseline the linear regression of the experimental data in the pre-denaturation region to obtain the excess (with respect the native state) molar heat capacity $C_P^{exc}(T)$ across the scanned temperature range. The heat capacity drop, $\Delta_d C_P$, across the signal was affected by a rather large error and was therefore not taken into account in the present work. The area underlying the recorded peaks, so treated, directly corresponds to the relevant denaturation enthalpy, $\Delta_d H°$, in $kJ \cdot mol^{-1}$ units. Errors were evaluated on the basis of at least three replicates. The fit attempts based on the denaturation thermodynamic models were accomplished using the nonlinear Levenberg-Marquardt method [77]. The errors of each fitting parameter were calculated with a 95.4% confidence limit by the Monte Carlo simulation method and resulted negligible with respect the experimental errors.

RESULTS AND DISCUSSION

In order to investigate whether or not the AgamOBP5 constitutes a novel protein target for repellent molecules, a preliminary *in vitro* screening of a number of compounds exhibiting repellent activity was performed by fluorescence competition assays. Synthetic repellents such as DEET, Icaridin, PMD, and IR3535, as well as known natural repellents belonging to linear and aromatic monoterpenes, were tested in one-point screening experiments at ligand concentrations of 5 and 10 μM (*data not shown*). Among the compounds tested, the two isomeric monoterpenoid phenols Carvacrol and Thymol were found to bind to AgamOBP5 with enhanced affinity. To gain structural and mechanistic insights into the features that govern their molecular recognition by the AgamOBP5, we performed binding studies both in solution and in the crystal state.

Fluorescence spectroscopy studies showed that Carvacrol and Thymol are strong AgamOBP5 binders

Following the initial screening for the identification of potential AgamOBP5 binders, a detailed fluorescence competition study of the most potent compounds Carvacrol and Thymol was performed in order to determine their specific binding characteristics. Fitting the fluorescence intensities to a one-binding-site saturation curve was deemed inadequate to interpret the obtained data, whereas a two-site model fits the experimental data very well. This outcome strongly suggests the presence of two binding sites on AgamOBP5 for both Carvacrol and Thymol molecules (**Figure 1).** We found that both Carvacrol and Thymol can bind to the first binding site of AgamOBP5 with high affinities in the submicromolar range (Ki=0.11 μM). However, the second binding site exhibits a significantly lower affinity for these compounds, showing dissociation constants of ~7 μM and ~18 μM for Carvacrol and Thymol, respectively (**Table 2**). The existence of two binding sites in AgamOBP5 is not unexpected given that OBPs bear large hydrophobic cavities and tunnels, therefore having the potential to accommodate more than a single copy of a ligand in their free available space. Specifically, our previous crystallographic, HSQC-NMR and calorimetric studies have shown that AgamOBP1 can simultaneously and selectively bind two Icaridin molecules in two distinct regions of its long hydrophobic tunnel [56]. We anticipate that this property of OBP proteins could be proven advantageous for the structure-based discovery of novel host-seeking disruptors, as will be discussed later in this work (*vide infra*).

Based on the data analysis suggesting the presence of high- and low-affinity sites in nearly equal proportions, (45:55), we estimated (see Y calculation - Supplemental material) that under the experimental conditions used, the high-affinity site (*referred from now on as "**Site-1**"*) is almost fully occupied (PL/P=99%) by the ligand at a concentration of 15 μM

(L/P=7.5). For the same L/P ratio, the low-affinity binding site (*hereinafter to be referred as* ***"Site-2"***) was calculated to be 65% and 44% occupied by Carvacrol and Thymol, respectively. Similarly, for an L/P ratio of 15, Site-2 occupancies by Carvacrol and Thymol rise to 81% and 61%, respectively, while they further increase to 93% and 85% at the maximum concentration used in our assays (100 μM ligand; L/P=50). While the dissociation constants of compounds for Site-2 are relatively low, it is remarkable that AgamOBP5 can discriminate, in terms of ligand transfer capacity, between the two structurally similar terpene isomers by exploiting a second site, which in all likelihood act as a reservoir for the excess of the ligand. Based on the above results, we may suggest that although AgamOBP5 detects Carvacrol and Thymol at low spatial concentrations with the same sensitivity, at high ligand concentrations mediates the transfer of extra Carvacrol rather than Thymol molecules to its cognate Odorant Receptor(s). Indeed, previous *in vitro* repellent assays showed that Carvacrol and Thymol display similar repellence indices, as expected for isomeric molecules. Nevertheless, Carvacrol was equally effective as Thymol (or even slightly more effective than Thymol) at a lower dose (25 nmol/cm^2) than that of Thymol tested (31 nmol/cm^2) [78]. Therefore, our results further corroborate the idea that OBPs contribute to the overall observed extraordinary selectivity and sensitivity of the insect olfactory system. Although OBPs lack absolute specificity, the ability of some of these proteins to detect specific molecules has also been reported. As an example, AgamOBP1 was able to stereoselectively bind in the crystal the most active component (1R,2S-Icaridin) of Icaridin's equimolar diastereoisomeric mixture [56].

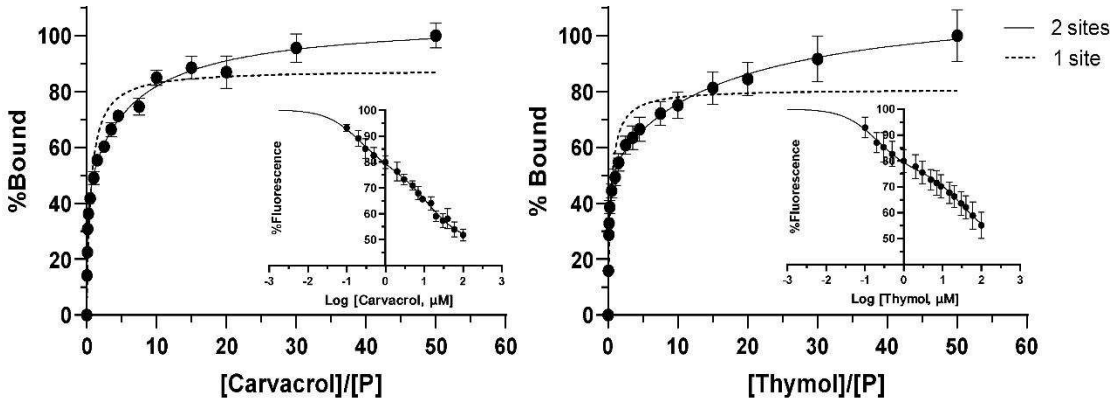

Figure 1. Fluorescence competition curves. Fluorescence data obtained with 2 µM AgamOBP5 at a constant concentration of 1-NPN (5 µM) and various concentrations of Carvacrol or Thymol (0-100 µM) (Supplemental **Tables S1** and **S2**). Fluorescence intensities were transformed to percentages of bound ligand (see Transformation - Supplemental material) and plotted with respect to the concentration fraction [L]/[P] (Total concentration of Ligand/Total Protein concentration; 2 µM). The [L]/[P] ratios at the half of maximum percentage of bound ligands were computed by employing the "Two sites-Specific binding" saturation model as implemented by Graphpad Prism Software (solid line). The corresponding "One site-Specific binding" curves are shown as dashed lines. ***(Insert)*** Dose-response curves showing the effect of Carvacrol and Thymol concentrations on the displacement of the fluorescent probe 1-NPN from AgamOBP5. The response was expressed as percentage of fluorescence reduction relative to the fluorescence observed at zero dose of ligand (100%). Dose-response data were plotted with respect to the logarithm of the ligand concentration (µM). The dissociation constants (Ki ± SEM) were calculated by employing the "Two sites - Fit Ki" model for Dose-response fitting under competitive conditions (5µM 1-NPN with Kd of 5.9 µM), as implemented by Graphpad Prism Software.

Table 2. Dissociation (*Ki*) and binding constants (Kb) of the tested compounds

Ligand	**Ki, µM ± SEM**		**[a][L]/[P] ± SEM**		**[b]K_b, M^{-1}**	
	Site		**Site**		**Site**	
	1	**2**	**1**	**2**	**1**	**2**
Carvacrol	0.11±0.03	7.26±1.62	0.11±0.02	6.74±1.45	8.77×10^6	13.8×10^4

Thymol	0.11±0.01	17.73±4.49	0.10±0.01	16.43±2.96	9.09×10^6	5.64×10^4

[a]Ligand/Protein concentration ratio at half-maximum binding according to the "Two sites-Specific binding" saturation model.

[b]1/Ki, M^{-1}

Calorimetric studies revealed that Carvacrol and Thymol induces a considerable protein stabilization

Differential Scanning Calorimetry was applied to assess the thermodynamic stability of the AgamOBP5 in solution and the effect of its interaction with the two ligands as suggested by the spectroscopic data (*vide supra*).

Figure 2 reports the calorimetric profile obtained for AgamOBP5, whereas the respective thermodynamic parameters are listed in **Table 3.** We observed a simple endothermic trace ascribable to the protein thermal denaturation. The application of thermal denaturation thermodynamic models [79-82] showed that the protein denaturation thermal profile is well described by a simple one-step native-to-denatured state equilibrium model

$$N \overset{K}{\leftrightarrow} U$$

as revealed by the best fit of theoretical vs experimental C_P^{exc} curve (**Figure 2**).

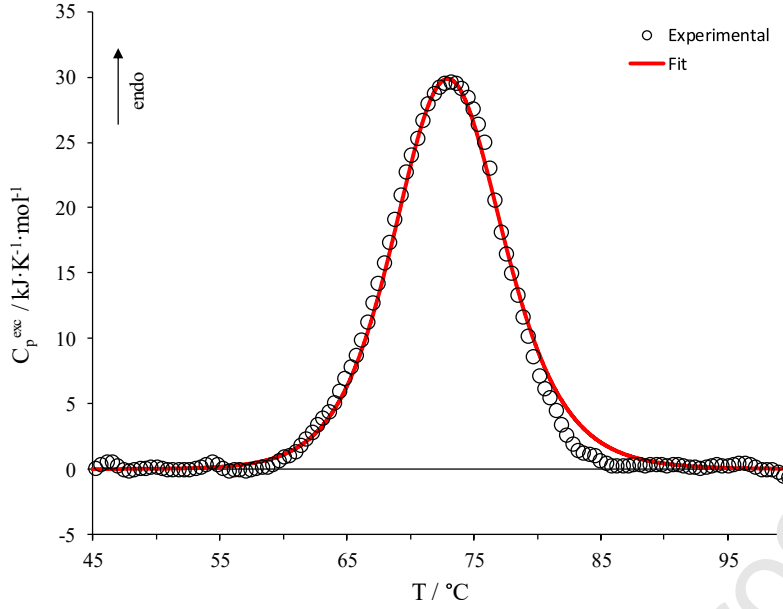

Figure 2. AgamOBP5 thermal denaturation. Nano-DSC thermogram obtained for AgamOBP5 thermal denaturation (black circles) and the respective theoretical curve calculated according to a one-step denaturation model (red curve). The calorimetric measurements were carried out at about 0.2 mM protein concentration in 10 mM Tris-HCl (pH 8.0) and 100 mM NaCl.

Table 3. AgamOBP5 denaturation thermodynamic parameters. Denaturation enthalpy, $\Delta_d H°$, and temperature, T_d, obtained by experimental DSC traces and best-fit values for samples of AgamOBP5 alone (without and with 2% methanol) and in the presence of Carvacrol and Thymol as ligands. The fit parameters were calculated according to a one-step denaturation model.

System	Experimental		One-step denaturation model Best-Fit parameters	
	$\Delta_d H°$ / kJ·mol^{-1}	T_d / °C	$\Delta_d H°$ / kJ·mol^{-1}	T_d / °C
AgamOBP5	330 ± 20	73.2 ± 0.5	345	73.0
AgamOBP5 + 2% Methanol (REF)	300 ± 20	71.8 ± 0.5	320	71.7
REF + Carvacrol ([L]/[P] = 7.5)	360 ± 20	75.9 ± 0.5	365	75.7

REF + Carvacrol ([L]/[P] = 15)	385 ± 20	78.1 ± 0.5	400	77.9
REF + Thymol ([L]/[P] = 15)	390 ± 20	78.1 ± 0.5	395	78.0

Nevertheless, to evaluate the effect of the interaction of AgamOBP5 with Carvacrol and Thymol, which were added from stock solutions in methanol (see materials and methods section), we need to consider the side effects deriving from the presence of methanol in solution in order to obtain a proper reference protein state. At our conditions, methanol concentration was always kept at 2% (v/v), hence its impact on protein's thermodynamics was evaluated at such a concentration (Supplemental **Figure S2** and **Table 3**). Methanol addition resulted in a slight destabilization of the protein as concerns both the denaturation enthalpy (Δ_dH^o) and temperature (T_d). Nonetheless, the presence of methanol did not affect the mechanism of denaturation, which was still a one-step equilibrium mechanism. This system was used as reference to compare the ligands effect.

The overall picture of the thermal stability of AgamOBP5 and its complexes with Carvacrol and Thymol ([L]/[P] = 15), *i.e.*, the maximum ligand-to-protein ratio compatible with our experimental conditions (see Materials and methods section), is reported in **Figure 3a**. According to the fluorescence data, this condition corresponds to a saturation of more than about 80% of the total binding sites for both Carvacrol- and Thymol-containing systems (about 90% and 80%, respectively).

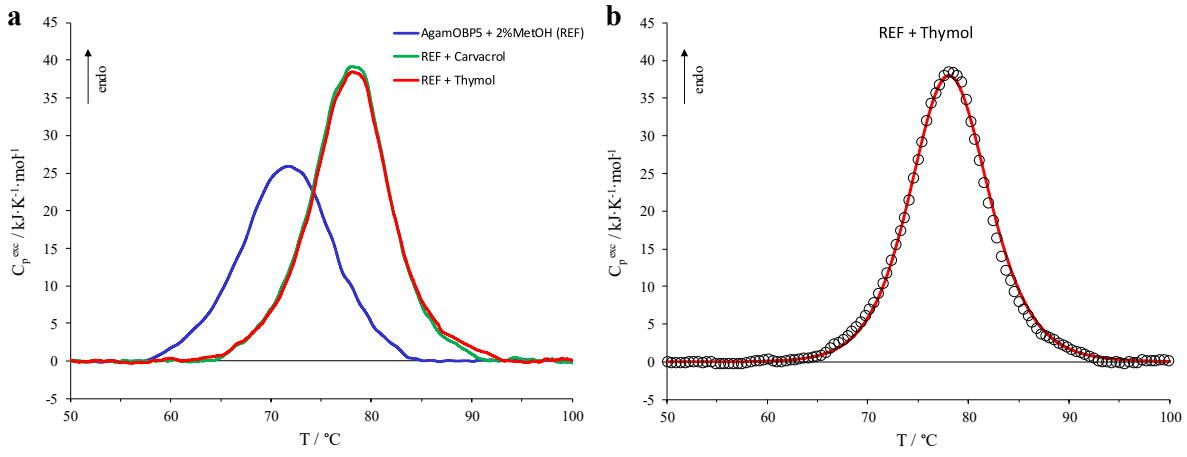

Figure 3. a) Denaturation profiles obtained for AgamOBP5 solution (2% (v/v) methanol) (blue trace) and for the protein in the presence of Carvacrol (green trace) and Thymol (red trace) at the same ligand-to-protein ratio ([L]/[P] = 15). **b)** Theoretical C_P^{exc} curve (red trace) obtained according to a one-step denaturation equilibrium model for Thymol at [L]/[P] = 15 (the black circles curve corresponds to the respective experimental nano-DSC profile).

It is evident that the interaction of the protein with both Carvacrol and Thymol induced a considerable protein stabilization against the denaturation process as concerns both the denaturation enthalpy, $\Delta_d H^o$, and temperature, T_d (**Table 3**). These effects are a clear indication of a specific ligand binding [79, 82] in accordance with the spectroscopic evidence.

In such a condition, we observe that the two ligands influenced the stability of the protein to a highly comparable extent. Moreover, the overall protein unfolding mechanism remained unaffected, still being fitted by a one-step denaturation model as shown in **Figure 3b** for AgamOBP5 in the presence of Thymol as an example (the respective curve for the Carvacrol-containing system is reported in the Supplemental **Figure S3**. Such an overall picture is in accordance with the very similar chemical structure of Carvacrol and Thymol as well as with the information obtained from the crystallographic data, which revealed no significant modifications in the overall protein tertiary structure upon the binding of the two ligands (*vide infra*).

Considering the high values of the binding constants K_b of both ligands for Site-1 obtained by spectroscopic methods (**Table 2**), and the indication that this high-affinity site is almost fully occupied at a [L]/[P] = 7.5, a trial was attempted at such condition for the Carvacrol system (Supplemental **Figure S3** and **Table 3**) in order to assess whether the modification of the protein thermal stability revealed by the calorimetric results at [L]/[P] = 15 is also due to the binding at Site-2. The results indicate a lower stabilization for such a system, suggesting that Carvacrol binding to Site-2 is also able to stabilize the protein.

The overall calorimetric picture reveals that the peculiarities emerged from the spectroscopic data, *i.e.*, very similar values for the ligands K_b at Site-1 and different but still same order values for their K_b at Site-2 (**Table 2**), do not result in significant differences of the protein thermal stability at [L]/[P] = 15.

Although it is well known that, in general, the variation of thermal stability of a protein due to specific binding progressively reaches a limit when the [L]/[P] ratio achieves values close to ligand saturation conditions [79, 83], we cannot exclude that such small differences in K_b values at Site-2 may become significant and calorimetrically detectable in any specific range of [L]/[P] ratios below saturation. However, these details do not change the overall picture and are beyond the scope of this work.

Overview of structural features of AgamOBP5

Initially, the crystal structure of AgamOBP5 was determined in the absence of ligands to a resolution of 1.35 Å (**Table 1**). AgamOBP5 belongs to the "classical" OBPs subfamily that displays a characteristic pattern of six conserved cysteines. Its globular structure consists of six α helices (α1-α6) connected by flexible loops that enclose a large central hydrophobic cavity. The long C-terminal tail of AgamOBP5 is directed toward the center of the protein, forming part of the cavity wall. Three conserved disulfide bridges that stabilize the compact protein structure, are formed between cysteine residues located in helices α1 and α3 (Cys18–Cys49), α3 and the start of helix α6 (Cys45–Cys102) and, α5 and the end of α6 helix (Cys91– Cys111). Other structural features of AgamOBP5 include two 3_{10} extensions of the α1 and α5 helices followed by their connecting loops with helices α2 and α6, respectively, a Hydrogen-bonded turn between α3 and α4 helices (Hb-turn), and the α2-α3 connecting loop bearing a FAED sequence (hereafter to be called FAED-loop) distinct from the corresponding one of its highly homologous protein AgamOBP4 (*vide infra* in comparison with AgamOBP4) (**Figure 4A**).

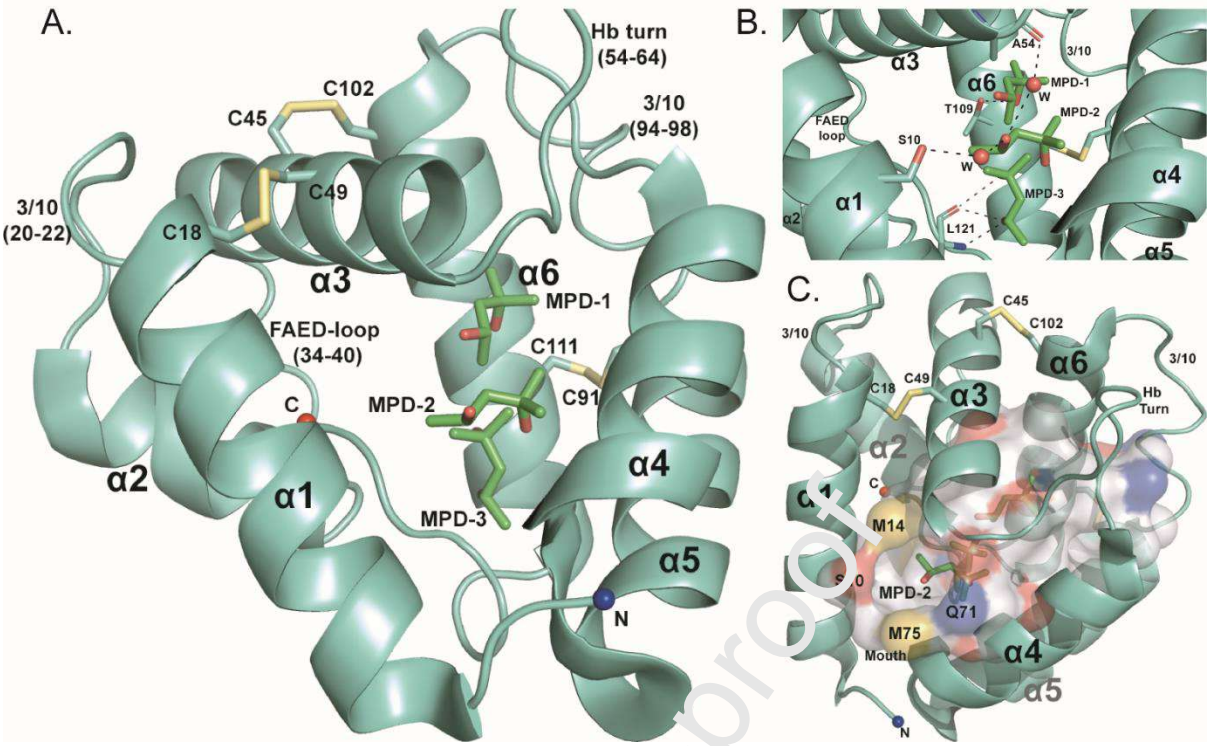

Figure 4. Overview of AgamOBP5 crystal structure. (A) Cartoon representation of AgamOBP5 with three MPD molecules bound in the central hydrophobic cavity. The three disulfide bonds are colored light orange. **(B)** MPD-1 and MPD-3 located at the bottom and the center of the binding cavity, respectively, forms direct hydrogen bonds to protein residues, whereas the MPD-2 molecule located at the cavity entrance participates in a hydrogen bonds network via two water molecules. Hydrogen bonds are shown as dashed lines. **(C)** Connolly molecular surface of the AgamOBP5 binding cavity showing the mouth opening between α1, α3 and α4 helices, occupied by the MPD-2 molecule.

The total volume of the central protein cavity is 247.81 $Å^3$, while its walls are comprised mainly by non-polar residues (68.75%) with a solvent-accessible surface area of 395.602 $Å^2$. his hydrophobic pocket is accessible to solvent through an opening on the protein surface of ~8.5 Å diameter, which is lined by the residues Ser10 and Met14 (α1 helix), Ala54 (α3 helix) and, Gln71 and Met75 (α4 helix) (**Figure 4C**).

Investigation of the AgamOBP5 structure obtained in the absence of ligands revealed that the central pocket is occupied by three MPD molecules derived from the crystallization

solution. Upon binding, the 2-hydroxyl group of MPD-1 molecule makes a polar contact with the OG1 atom of Thr109 of helix α6 (2.81 Å). he corresponding hydroxyl group of MPD-2 placed between helices α1 and α4 at the entrance of the opening to the cavity forms indirect polar contacts from its 2-oxygen atom to Ser10;OG (α1) and Ala54;O (α3) via two water molecules but is not involved in any direct polar interaction with the protein. The third MPD molecule (MPD-3) interacts through the same oxygen with the main-chain oxygen and nitrogen atoms of Leu121 belonging to the C-terminal segment (2.97 Å) (**Figure 4B**).

The structures of AgamOBP5•Carvacrol and AgamOBP5•Thymol crystal complexes

In order to investigate the molecular basis of Carvacrol and Thymol recognition by AgamOBP5, we performed co-crystallization experiments of AgamOBP5 with these compounds. The analysis of the obtained crystal structures revealed the binding of both ligands to the hydrophobic cavity of the protein target (**Figure 5**).

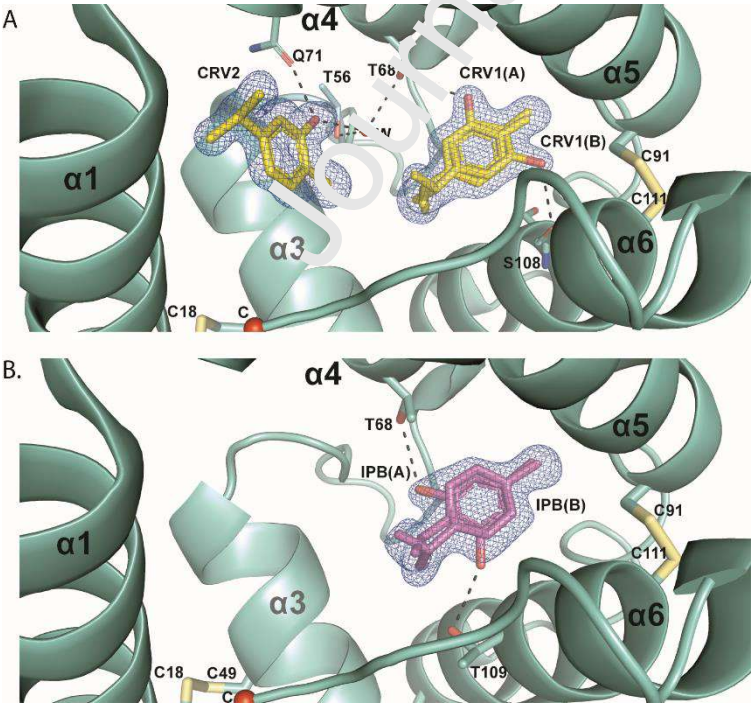

Figure 5. Electron density maps of the ligand molecules bound to AgamOBP5. The

molecules of (**A**) Carvacrol and (**B**) Thymol fitted into the 2*Fo*–*Fc* electron density maps of the final refined models contoured at 1σ. The polar interactions between ligands, protein residues, and a water molecule at the AgamOBP5 binding cavity, are shown as black dashed lines.

In the case of the AgamOBP5•Carvacrol complex, the initial F_o-F_c electron density map indicated the presence of three positive peaks inside the cavity, overlaid by 2*Fo*-F_c electron density map contoured at 1.0σ. The electron density of two of the three peaks closely resembled the molecular shape of Carvacrol, therefore, two ligand molecules were fitted into the map (**Figure 5A**). The third electron density peak was assigned to an MPD molecule, originating from the crystallization condition. In this position, it fully overlaps with the MPD-3 molecule (Supplemental **Figure S4)** of the monoterpene-free protein structure.

The first Carvacrol's binding site on AgamOBP5 (**Site-1**) is located at the bottom of the central cavity, between helices α4 and α5, and is bordered by helix α5. In this site, the position of its phenolic hydroxyl group appears not to be unique, suggesting the existence of two alternate ligand conformations. Indeed, further refinement of each of the two alternate conformations resulted in a negative F_o-F_c peak for the hydroxyl group, accompanied by an additional positive density peak at the opposite ortho-position of the phenolic ring. Therefore, two distinct Carvacrol conformations (CRV1-A and CRV1-B), related by a 180° rotation, were modeled into the density, each with half occupancy. Comparison with the unliganded AgamOBP5 structure showed that the Carvacrol molecule of Site-1 partially overlaps with the MPD-1 molecule (Supplemental **Figure S4**).

The second molecule of Carvacrol (CRV2) is found bound to a site (**Site-2**) localized near the opening of the protein cavity, at a position where it partially overlaps with MPD-2 (Supplemental **Figure S4**) of the AgamOBP5 monoterpene-free structure. In contrast to the CRV1 molecule, the position of Carvacrol's 2-hydroxyl group at Site-2 is well-defined, thus demonstrating its binding as a single conformer.

Upon binding to Site-1 of AgamOBP5, Carvacrol forms two hydrogen bonds through its

2-hydroxyl group to Thr68 of α4 helix (CRV1-A) and the main chain oxygen of Ser108 belonging to helix α6 (CRV1-B), and 34 van der Waals (vdW) interactions to atoms of the cavity (or 37 for CVR1-B including one with the CRV2 molecule in Site-2) (Supplemental **Table S3.A.** and **Figure 6A & 6B**).

Respectively, in Site-2, the hydroxyl oxygen atom of Carvacrol is hydrogen-bonded to Gln71 of α4 helix while also participating in water-mediated bridges with the side chain oxygens of Thr56 (loop α3-α4) and Thr68 of helix α4. Furthermore, Carvacrol CRV2 makes 31 additional vdW contacts, including six ligand-ligand interactions, one with the CRV1-B of Site-1, three with the MPD-3, and two with an S-1,2-Propanediol molecule (Supplemental **Table S3.B.** and **Figure 6C**).

The analysis of the AgamOBP5-Thymol complex structure showed that the Thymol molecule occupies only Site-1, where it binds in a position that perfectly overlaps with the one of Carvacrol (**Figure 5B**). Similar to Carvacrol, the Thymol molecule adopts two alternative conformations, IPB-A and IPB-B, which were refined with occupancies of 0.6 and 0.4, respectively. Thymol makes hydrogen bonds through its OH group to Thr68 of helix α4 (IPB-A) and Thr109 of α6 (IPB-B), and 28 van der Waals interactions to residues of the cavity (or 29 for IPB-B). The interactions of both ligands with the protein residues and other molecules are depicted in **Figure 6** and summarized in Supplemental **Tables S3** and **S4.**

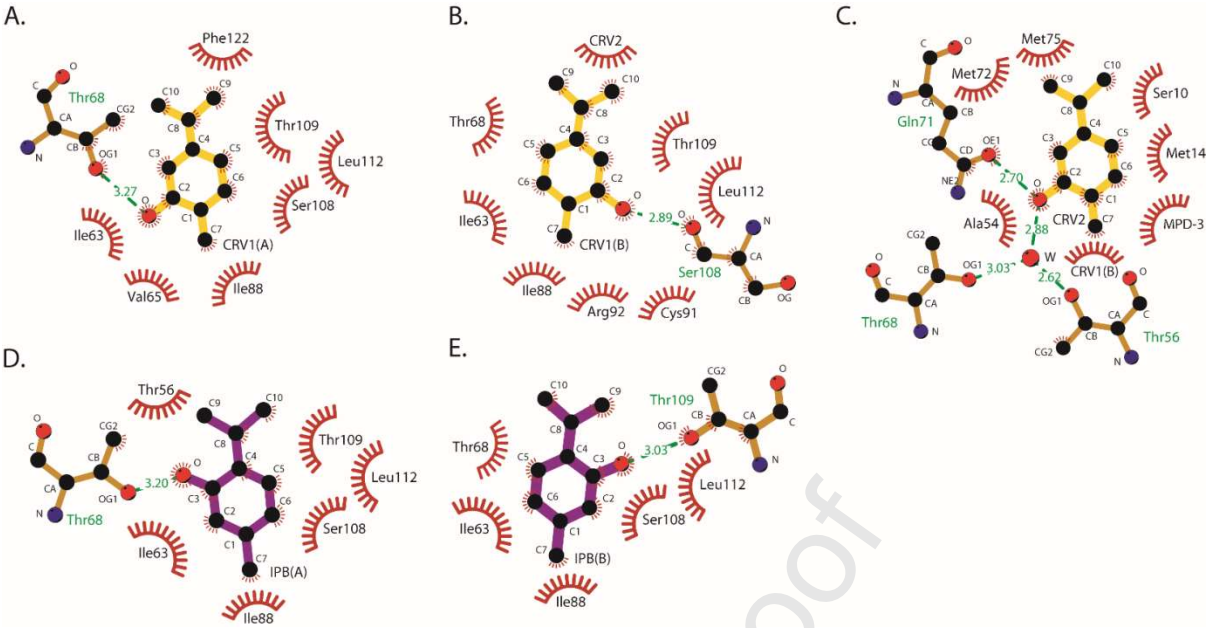

Figure 6. Schematic diagram (LigPlot) of Protein-Ligand interactions. (**A, B**) Diagram of Carvacrol bound to Site-1, in two alternative overlapping conformations CRV1-A and CRV1-B, and (**C**) Carvacrol in Site-2 as a single conformer (CRV2). (**D, E**) The corresponding diagram of the Thymol overlapping conformers (IPB-A and IPB-B) bound to Site-1. The hydrogen bonds are represented as green dashed lines. The van der Waals contacts are depicted as red semi-circles by radiating spokes. For figure simplicity only protein residues within a 3.9Å distance from the ligand are shown (for a detailed list of contacts within 4Å of the ligands see Supplemental **Tables S3** and **S4**).

Consistent with the fluorescence spectroscopy studies, the crystallographic results clearly confirmed the existence of at least two binding sites (Site-1 and 2) and a potential third one (MPD-3 Site), each with different local environments. Although Thymol was not found bound to Site-2 at the determined crystallographic complex, we cannot exclude its binding in solution state under the experimental conditions of fluorescence and DSC experiments, *i.e.*, in the absence of competitors and use of totally unliganded (MPD-free) protein. Furthermore, given the lower affinity of Thymol for Site-2, compared to that of Carvacrol (see fluorescence spectroscopy section), it is possible that Thymol's saturation (occupancy) for Site-2 may not have been high enough under the experimental conditions of our co-crystallization studies in order to observe its binding to the crystal. Unfortunately,

attempts to increase the Thymol concentration in soaking or co-crystallization experiments resulted in either ligand precipitation or crystal distortion and failure of crystal growth, respectively, due to the increased organic solvent content.

In the absence of an MPD-free AgamOBP5 structure, any potential changes in the overall tertiary structure that promote protein stabilization, as observed in the DSC experiments, are difficult to conclude. Nevertheless, it is clear that both Carvacrol and Thymol at Site-1 bridge the α4 and α6 helices via hydrogen bonding and further interact with helix α5 through vdW contacts. Moreover, the Carvacrol molecule at Site-2 extends this network of interactions to the end of the α3 helix. While the crystal structure of the AgamOBP5-Thymol complex did not reveal the binding mode of Thymol in Site-2, we could suggest that its binding may resemble that of Carvacrol, participating as well in an extended network of interactions among α4, α5, α6, and α3 helices. This suggestion is further supported by our DSC results which show that both ligands stabilize the protein to the same extent.

The formation of an extended network of interactions between ligands and protein residues, including structural waters, could further result in the intertwining of the helices, concerted motions of structural domains, propagation of the interactions to distant regions (allosteric effect), and thus in the overall stabilization of protein structure. Specifically, previous HSQC-NMR experiments showed that the binding of indole on the highly homologous AgamOBP4 protein induces its structural transition from a molten globule state to a well-folded form and further mediates the formation of a distant binding site for AgamOBP1 through allosteric changes, thereby promoting their heterodimerization [84].

Structural comparison between the crystal complexes of AgamOBP5

The comparative analysis of the obtained AgamOBP5 crystal structures revealed that

the binding of Carvacrol and Thymol to AgamOBP5 does not accompany by significant conformational changes in the overall tertiary structure of the protein compared to the MPD complex. The overall root-mean-square deviation (RMSD) of the backbone atoms of AgamOBP5-Carvacrol, AgamOBP5-Thymol, and AgamOBP5-MPD structures are 0.522Å and 0.23Å, respectively, with the AgamOBP5-Thymol complex to resemble more closely the structure with MPD. The main backbone atom differences (RMSD >1 Å) are observed at residues 54-57 of the Hb-turn loop region located between helices α3 and α4, residues 74-79 of the α4-α5 connecting loop, and residue 93 belonging to the 3_{10} helix extension of α5 (**Figure 7A**).

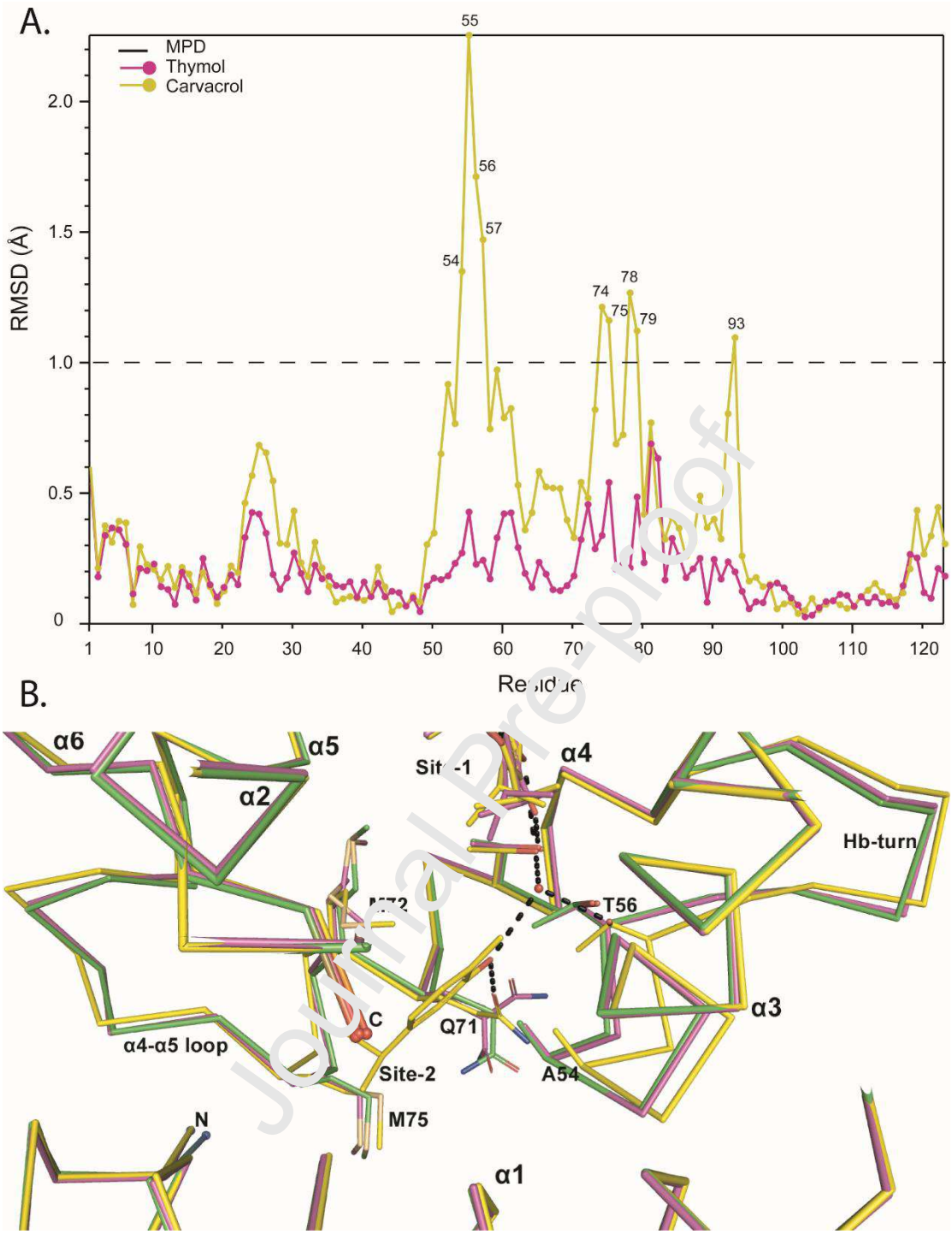

Figure 7. Structural comparison of ligands complexes. (A) RMSD per residue. Plot of the r.m.s. deviation (RMSD) of main-chain coordinates of the Carvacrol (yellow) and Thymol (magenta) complexes, with the reference MPD complex. Residues with shifts greater than 1Å are indicated. **(B)** The Carvacrol binding Site-2 in AgamOBP5. Structure superimposition of AgamOBP5-Carvacrol complex (yellow) and AgamOBP5-Thymol complex (magenta) onto the MPD-bound structure (green) showing the major conformational changes occurred upon the binding of ligands. The Site-2 is

delineated by α1, α3, α4 helices and the C-terminal residue Pro123 of α6 helix.

Comparison of Carvacrol and Thymol complexes with the MPD structure revealed that the Site-1 region undergoes very few conformational changes (Supplemental **Figure S6**). The only exception is found in the main chain of Asp93 of the AgamOBP5-Carvacrol complex. However, its side chain is not part of the binding cavity interior but is exposed to the bulk solvent in all the obtained ligand complexes. This finding suggests that Site-1 may be a preformed high-affinity binding site for both compounds, Carvacrol and Thymol. Their binding can additionally stabilize the relative positions of the site's surrounding α4, α5, and α6 helices without requiring high energy consumption for their structural rearrangement.

In the AgamOBP5-Carvacrol structure, residues 54-57 of the Hb-turn (α3-α4 loop) shift away from the CRV2 molecule so as to facilitate the establishment of a water-mediated interaction between the side-chain hydroxyl group of Thr56 and the hydroxyl oxygen of ligand (**Figure 7B**). In contrast, the position of this water molecule is occupied by the side chain of Thr56 in both Thymol and MPD structures. A significant displacement was also observed for the main chain atoms of Ala54 away from Carvacrol, which optimized the vdW interactions of its Cβ atom with the ligand's aromatic ring (**Figure 7B** and Supplemental **Table S3.B.**). In addition, a perturbation in the 74-79 residues region of the α4-α5 connecting loop, results in the shift of the main chain atoms of Met75 by ~1Å away from the CRV2 molecule in order to optimize the vdW contacts between its SD atom and the isopropyl moiety of the ligand.

Furthermore, the occupation of Site-2 by Carvacrol also triggers side-chain rearrangements. Specifically, the side chain of Gln71 is displaced from its position in the MPD complex where it is exposed to the solvent, towards Carvacrol. In this position, it participates in a direct hydrogen bond with Carvacrol's hydroxyl group. In contrast, in the AgamOBP5-Thymol complex, where Site-2 is unoccupied, Gln71 is found in both alternative

conformations. Likewise, the side chain of Met72 enters the binding Site-2 inducing numerous vdW interactions with the isopropyl and hydroxyl groups, as well as the aromatic ring of Carvacrol.

Residues Ala54, Met75, and Gln71 contribute to the formation of the mouth opening into the internal cavity, which becomes more hydrophobic during the transition from the MPD complex to the Thymol and the Carvacrol one due to their structural adaptability (Supplemental **Figure S5**).

In conclusion, the ligand binding to the low affinity binding Site-2 requires several conformational changes of both the main and side chains of the adjacent protein residues. Furthermore, Site-1 displays fewer energetic restrictions on the position of the ligand found bound in two alternative binding modes in both complexes. This finding may explain the lower affinity of Site-2 compared to the preformed Site-1, by means of the required energetic cost. An additional explanation for the significantly lower affinity of Site-2 could be the lower number of interactions developed by the single molecule, compared to those made by the two alternative binding modes of the ligand in Site-1.

The difference in the binding affinity of Carvacrol and Thymol for Site-2, determined from the fluorescence experiments, cannot be structurally explained by the available crystal structures. It is possible that the ortho position of Thymol's hydroxyl group is less effective in forming the critical hydrogen bonds with Gln71 and the bridging water molecule, observed in the Carvacrol complex. Nevertheless, we propose that the binding of a second molecule, either Carvacrol or Thymol, further stabilizes the overall structure as revealed by our DSC experiments and, in agreement with the crystallographic evidence. It should be noted that the AgamOBP5-MPD complex is not an ideal representative of the apo-protein form as both binding sites are occupied by MPD molecules. However, MPD-1 cannot act as a bridge between α4 and α6 helices suggesting that the relative positions of α4 and α6 are pre-adopted and not affected by the ligand binding. Respectively, MPD-2 cannot be water-

bridged to either α3 or MPD-1, suggesting that the structural changes in Site-2 are induced by the binding of the second monoterpene molecule (**Figure 4B**). Interestingly, structural comparison showed that in the Thymol complex a number of Site-2 residues such as Gln71 and Met72, adopt two alternative conformations, one of which overlays with the single conformation observed in the Carvacrol and MPD structures, respectively (**Figure 7B**). This further indicates that under the given crystallization conditions, Thymol also interacts, though to a low extent, with Site-2 despite the fact that its concentration was not sufficient to saturate this crystal site and be observed co-crystallized.

Structural comparison of AgamOBP5 with the AgamOBP4-Indole complex

The AgamOBP5 sequence shows 62% identity and 73% similarity (positives) to the AgamOBP4 protein (Supplemental **Figure S7**). The binding of Indole to AgamOBP4 has been linked to the formation of the AgamOBP1-OBP4 heterodimer [84]. Herein, a structural comparison of these highly homologous proteins was performed in order to better understand the molecular basis of their specificities.

The overall root-mean-square deviation (RMSD) of Cα and backbone atoms between the AgamOBP5 and AgamOBP4 structures are 3.748Å and 3.351 Å, respectively, with the α2 helix (25-33) and the following FAED-loop (34-40) exceeding the value of 4 Å in average.

AgamOBP4 contains two additional proline residues in the so-called FAED-loop connecting the α2 and α3 helices. In particular, in the AgamOBP4 structure, the segment of the α2-α3 loop comprising the residues 37 to 42 (F**P**AN**P**D) has been replaced in AgamOBP5 by the shorter sequence segment FAED (aa 37-40) (Supplemental **Figure S7**). Overall, the loop (aa 34-40) adopts an opposite orientation in the two protein structures. As a result, Ala38 of AgamOBP5 is oriented toward the α2 helix, while the corresponding alanine residue in the AgamOBP4 structure is exposed to the bulk solvent (**Figure 8A and** Supplemental

Video). Furthermore, in the AgamOBP5-Carvacrol complex, Glu39 makes two hydrogen bonds, through its OE1 and OE2 atoms, with Tyr107;OH of the α6 helix and a salt bridge (3.2 Å) to Lys44;NZ of helix α3, thus further stabilizing the protein structure through the α3-α6 interconnection (**Figure 8B**). Additional amino acid substitutions and their interactions are described in the Supplemental **Figure S8.**

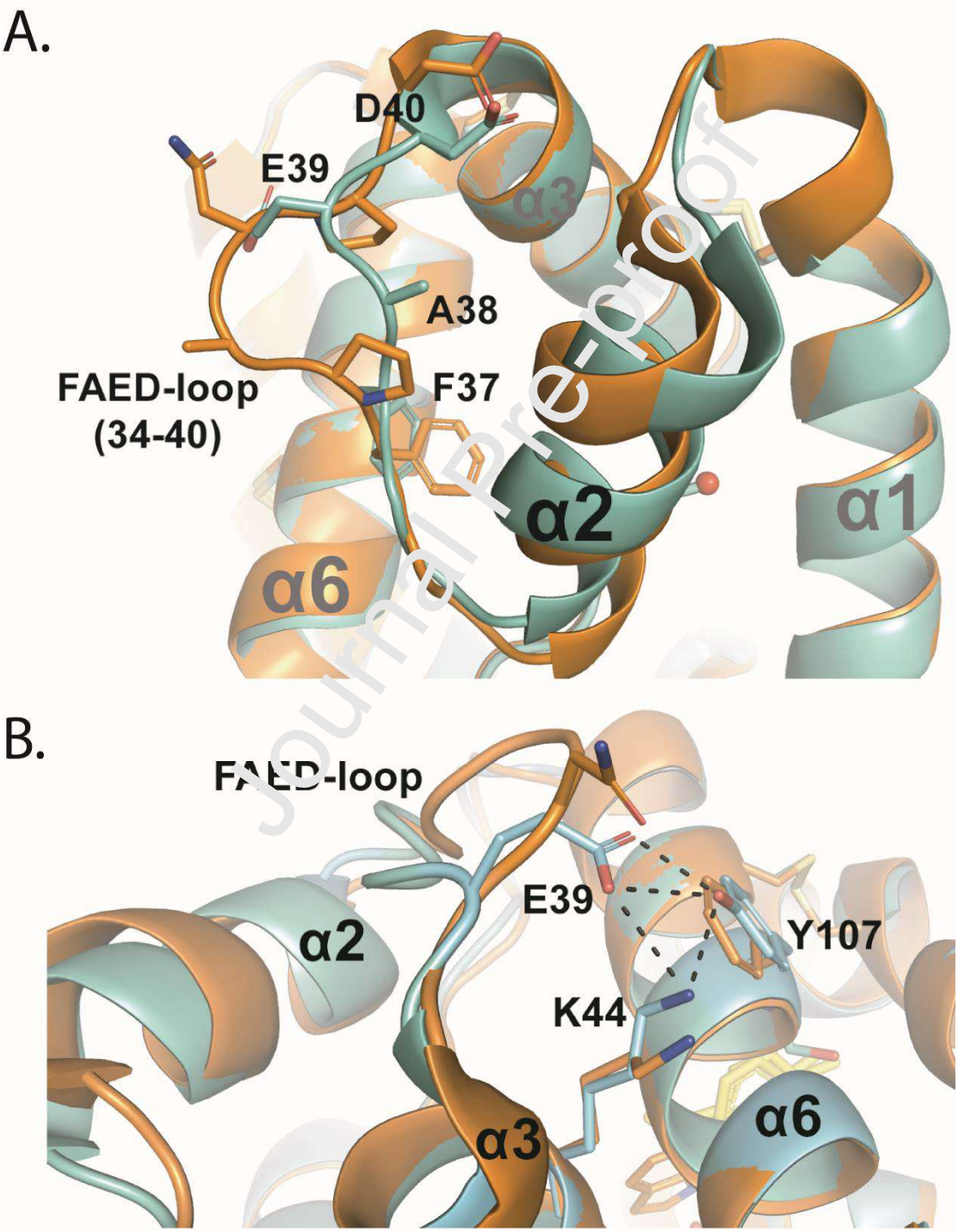

Figure 8. Structural comparison between AgamOBP5 and AgamOBP4 in the FAED-loop

region. (A) Superimposition of AgamOBP5 (green) onto the AgamOBP4 (orange) structure, showing the major conformational differences observed in the FAED-loop and α2 helix.

Superposition of the acquired AgamOBP5 structures with the AgamOBP4-indole complex (PDB id: 3Q8I) showed that the indole molecule localizes in a region between the binding Site-1 and Site-2 of AgamOBP5 (**Figure 9A**). At this position, indole perfectly overlaps with the MPD-1 molecule of the AgamOBP5-MPD complex (**Figure 4A-B** and Supplemental **Figure S9**).

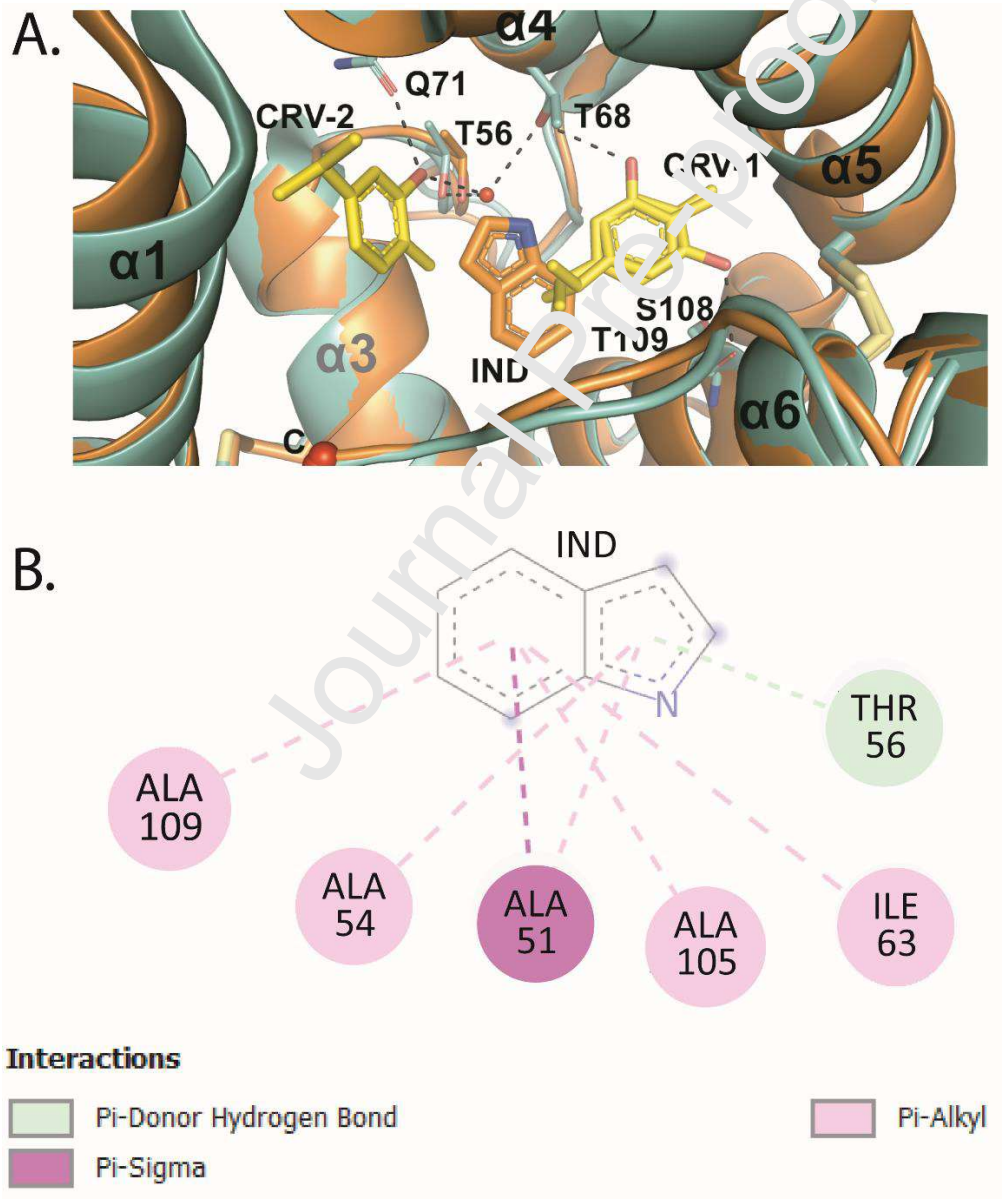

Figure 9. Comparison of Carvacrol and Indole binding sites and modes. (A) Superimposition

of AgamOBP5-Carvacrol (yellow) and AgamOBP4-Indole (orange) complexes. Indole is placed in a location where it partially overlaps with the isopropyl group of Carvacrol CRV1 in Site-1. In this position it is perfectly overlaps with the MPD-1 molecule of AgamOBP5-MPD complex (see Figure 4A-B). **(B)** 2D-diagram, showing π-interactions of Indole bound to AgamOBP4. Protein residues within 3.9 Å of the ligand are indicated. Indole's aromatic ring can act as a proton acceptor to form a π-hydrogen bond with Thr56 OG1. In contrast to Carvacrol or Thymol when bound to AgamOBP5, indole does not form any conventional hydrogen bond to residues of AgamOBP4.

Upon binding to AgamOBP4, Indole makes a total of 31 vdW contacts, similar in number to those of each individual conformation of Carvacrol or Thymol (Supplemental **Tables S3** and **S4**). However, in the crystal structure reported by Davrazou et al. [84], indole has been modeled with partial occupancy (O=0.6) in the vicinity of the AgamOBP4 cavity. In addition, indole was found to make only one π-hydrogen bond with Thr56 (3.22 Å) (**Figure 9B**) and a distant polar vdW interaction, through its aromatic nitrogen, to the OH group of Thr68 (3.62 Å). These findings demonstrate the existence of considerable flexibility of the indole in the AgamOBP4 binding site. In contrast, the monoterpene molecules in this work were refined with full occupancy (the sum of the occupancies is equal to 1) and found to participate in a network of potential hydrogen bonds with residues that could be considered anchor points for the binding of ligands to AgamOBP5.

With the exception of the residue variations A109T, F65V, and A105T, the aminoacids lining the binding Site-1 and Site-2 of AgamOBP5 are similar, *i.e.*, L88I, A112L, and I72M, or identical in AgamOBP4 (Supplemental **Figure S7**). Significantly, in the region of the AgamOBP5 Site-1, Thr109 replaces an Alanine residue of AgamOBP4. The hydroxyl group of Thr109 forms a hydrogen bond with Thymol and additional vdW interactions with both Thymol and Carvacrol (**Figure 5** and Supplemental **Tables S3** and **S4**). In contrast, its counterpart residue Ala of AgamOBP4 makes only one long-range vdW contact (3.96 Å) with the bound Indole molecule. Furthermore, AgamOBP4 Ala112 is substituted in AgamOBP5 by

the longer side chain residue Leu112, which constitutes a significant source of vdW interactions with both Carvacrol and Thymol molecules. In addition, Ile72 of AgamOBP4 is replaced by the longer side chain residue Met72 that participates in a number of vdW interactions with Carvacrol CRV2 at Site-2. In the binding site of AgamOBP4, the short non-polar side chain of Ala105 which is involved in a π-alkyl interaction with indole, is substituted by the long polar side chain of Thr105. These variations lead to binding cavities of different chemical environment, shape, and volume, and consequently of different binding specificities. Replacement of hydrophobic residues of the binding pocket by others with longer side chains further limits the size of recognizable hydrophobic ligands. Thr109 found to be essential for Thymol's binding to Site-1 would obstruct the binding of indole to AgamOBP5 due to steric clashes. AgamOBP5 may be more specific for monocyclic compounds rather than bulkier polycyclic aromatic molecules like indole. Our detailed structural analysis at the residue level suggests different binding specificities for AgamOBP4 and AgamOBP5. Therefore, provides a plausible answer to the reasonable question about the need for the existence of two highly homologous and similarly folded proteins in the mosquito olfactory system. Moreover, at the level of tertiary structure, the differences observed in the orientation of the FAED-loop, the α2 helix, and the segment connecting the α4 and α5 helices of AgamOBP5, could result in the formation of an additional distinct site suitable for heterodimers generation as AgamOBP4 does, further extending the number of detectable chemical cues. The potential of AgamOBP5 to form heterodimers with other OBPs possessing different binding specificities remains to be investigated in future studies.

Conclusion

Herein, we reported the first crystal structure of AgamOBP5 and its complexes with the natural plant repellents Carvacrol and Thymol at atomic resolution, and furthermore, we

revealed their binding characteristics in solution. Structural elucidation of novel OBP targets contributes to a deeper understanding of the mechanisms underlying the molecular recognition of semiochemicals by the OBPs. The obtained biochemical and structural information, combined together, increases the repertoire of available targets that can be used in the exploration of the available chemical space through structure-based approaches toward the discovery of new potent agents as potential mosquito host-seeking disruptors. Virtual and binding screening against libraries of natural compounds could reveal several novel AgamOBP5 binders.

The presence of alternative conformations of ligands upon their binding to Site-1 paves an exciting way for the design of bioinspired compounds featuring combined "olfactophore" characteristics, like substituted ortho- and meta-monoterpene analogs incorporating the alternative conformations in a single molecule. In addition, the existence of at least two binding sites on AgamOBP5 enables the design of conjugated molecules capable of simultaneously occupying both Sites 1 and 2.

As we have mentioned, the lower affinity Site-2 could act as a ligand's reservoir and possibly be involved in the concentration-dependent recognition mechanism of Carvacrol over Thymol. Nevertheless, we cannot exclude the existence of a yet unknown natural volatile molecule or a pheromone (ligand-X) with much higher affinity and specificity for Site-2 rather than Site-1. In that case, the co-existence of the two sub-sites, 1 and 2, could serve the detection of signature mixtures containing both Carvacrol or Thymol and Ligand-X. Alternatively, future studies could lead to the identification of a natural AgamOBP5-specific molecule long enough to occupy the full-length tunnel from mouth to bottom, thus interacting with both sub-sites and exhibiting a very high overall affinity. As an analogous example, the MOP pheromone was found to occupy a large segment of the CquiOBP1 tunnel and to partially overlap with both Icaridin sub-sites [56, 85].

Whereas at first glance the existence of two structurally similar and highly homologous

proteins, such as AgamOBP4 and AgamOBP5, seems to oppose the molecular economy of nature, our structural comparison provides a molecular explanation on how two structurally alike proteins have disparate specificity profiles. This structural resemblance could be exploited for the structure-based design of molecules that can bind to both AgamOBP4 and AgamOBP5 proteins, thus affecting more than one Odorant Receptor at the same time. Given that only two OBP crystal complexes with repellent molecules have been resolved so far *i.e.*, AgamOBP1 with the synthetic DEET and Icaridin, we anticipate that the introduction of novel OBP structures and of their complexes with volatiles of divergent chemical classes into *in silico* approaches will greatly facilitate the discovery of novel repellents of high efficacy and favorable safety profile.

Acknowledgments

This study was supported by European Regional Development Fund of the EU and Greek national funds through the Operational Program Competitiveness, Entrepreneurship and Innovation-call RESEARCH, CREATE, INNOVATE (QFytoTera, T1EDK-00996). This work was also supported by a fellowship to P.G.A. by the Hellenic State Scholarships Foundation and the action "Support of human research resources through doctoral research" funded by the "Operational Programme Education and Lifelong Learning" co-funded by the European Social Fund (ESF) and National Resources, MIS5000432. Access to European X-rays infrastructures has been supported by iNEXT (GA-653706) and iNEXT-Discovery (GA-871037), funded by the Horizon 2020 program of the European Commission. The authors would like to thank Diamond Light Source for beamtime (proposals MX22891 and MX18136), and the staff of beamlines I03 and I04-1 for assistance with crystal testing and data collection.

References

1. WHO: World malaria report 2021. https://www.mmv.org/sites/default/files/uploads/docs/publications/World_Malaria_Report_2021.pdf, Accessed December 2022

2. Chareonviriyaphap T, Bangs MJ, Suwonkerd W, Kongmee M, Corbel V, Ngoen-Klan R. Review of insecticide resistance and behavioral avoidance of vectors of human diseases in Thailand. Parasit Vectors. 2013;6:280. https://doi.org/10.1186/1756-3305-6-280
3. Debboun M, Strickman D. Insect repellents and associated personal protection for a reduction in human disease. Medical and Veterinary Entomology. 2013;27(1):1-9. https://doi.org/10.1111/j.1365-2915.2012.01020.x
4. Norris EJ, Coats JR. Current and Future Repellent Technologies: The Potential of Spatial Repellents and Their Place in Mosquito-Borne Disease Control. International Journal of Environmental Research and Public Health. 2017;14(2). https://doi.org/10.3390/Ijerph14020124
5. Briassoulis G, Narlioglou M, Hatzis T. Toxic encephalopathy associated with use of DEET insect repellents: a case analysis of its toxicity in children. Human & Experimental Toxicology. 2001;20(1):8-14. https://doi.org/10.1191/096032701676731093
6. Corbel V, Stankiewicz M, Pennetier C, Fournier D, Stojan J, Girard E, et al. Evidence for inhibition of cholinesterases in insect and mammalian nervous systems by the insect repellent deet. Bmc Biology. 2009;7:-. https://doi.org/10.1186/1741-7007-7-47
7. Legeay S, Clere N, Hilaire S, Do QT, Bernard P, Quignard JF, et al. The insect repellent N,N-diethyl-m-toluamide (DEET) induces angiogenesis via allosteric modulation of the M3 muscarinic receptor in endothelial cells. Scientific Reports. 2016;6. https://doi.org/10.1038/Srep28546
8. Astroff AB, Freshwater KJ, Young AD, Stuart BP, Sangha GK, Thyssen JH. The conduct of a two-generation reproductive toxicity study via dermal exposure in the Sprague-Dawley rat - A case study with KBR 3023 (a prospective insect repellent). Reproductive Toxicology. 1999;13(3):223-32
9. Klun JA, Strickman D, Rowton E, Williams J, Kramer M, Roberts D, et al. Comparative resistance of Anopheles albimanus and Aedes aegypti to N,N-diethyl-3-

methylbenzamide (Deet) and 2-methylpiperidinyl-3-cyclohexen-1-carboxamide (AI3-37220) in laboratory human-volunteer repellent assays. J Med Entomol. 2004;41(3):418-22

10. Pellegrino M, Steinbach N, Stensmyr MC, Hansson BS, Vosshall LB. A natural polymorphism alters odour and DEET sensitivity in an insect odorant receptor. Nature. 2011;478(7370):511-4. https://doi.org/10.1038/nature10438
11. Stanczyk NM, Brookfield JFY, Ignell R, Logan JG, Field LM. Behavioral insensitivity to DEET in Aedes aegypti is a genetically determined trait resulting in changes in sensillum function. Proceedings of the National Academy of Sciences of the United States of America. 2010;107(19):8575-80. https://doi.org/10.1073/pnas.1001313107
12. Stanczyk NM, Brookfield JFY, Field LM, Logan JG. Aedes aegypti Mosquitoes Exhibit Decreased Repellency by DEET following Previous Exposure. Plos One. 2013;8(2). ARTN e54438 https://doi.org/10.1371/journal.pone.0054438
13. Kröber T, Koussis K, Bourquin M, Tsitsura P, Konstantopoulou M, Awolola TS, et al. Odorant-binding protein-based identification of natural spatial repellents for the African malaria mosquito Anopheles gambiae. Insect Biochem Mol Biol. 2018;96:36-50. https://doi.org/10.1016/j.ibmb.2018.03.008
14. Odalo JO, Omolo MO, Malebo H, Angira J, Njeru PM, Ndiege IO, et al. Repellency of essential oils of some plants from the Kenyan coast against Anopheles gambiae. Acta Trop. 2005;95(3):210-8. https://doi.org/10.1016/j.actatropica.2005.06.007
15. Omolo MO, Okinyo D, Ndiege IO, Lwande W, Hassanali A. Repellency of essential oils of some Kenyan plants against Anopheles gambiae. Phytochemistry. 2004;65(20):2797-802. https://doi.org/10.1016/j.phytochem.2004.08.035
16. Asadollahi A, Khoobdel M, Zahraei-Ramazani A, Azarmi S, Mosawi SH. Effectiveness of plant-based repellents against different Anopheles species: a systematic review. Malaria Journal. 2019;18(1):436. https://doi.org/10.1186/s12936-019-3064-8

17. Ignell R, Hill SR. Malaria mosquito chemical ecology. Curr Opin Insect Sci. 2020;40:6-10. https://doi.org/10.1016/j.cois.2020.03.008

18. Wooding M, Naude Y, Rohwer E, Bouwer M. Controlling mosquitoes with semiochemicals: a review. Parasit Vectors. 2020;13(1):80. https://doi.org/10.1186/s13071-020-3960-3

19. Leal WS. Odorant reception in insects: roles of receptors, binding proteins, and degrading enzymes. Annu Rev Entomol. 2013;58:373-91. https://doi.org/10.1146/annurev-ento-120811-153635

20. Vogt RG, Riddiford LM. Pheromone Binding and Inactivation by Moth Antennae. Nature. 1981;293(5828):161-3. https://doi.org/10.1038/293161a0

21. Qiao H, Tuccori E, He X, Gazzano A, Field L, Zhou JJ, et al. Discrimination of alarm pheromone (E)-beta-farnesene by aphid odorant-binding proteins. Insect Biochem Mol Biol. 2009;39(5-6):414-9. https://doi.org/10.1016/j.ibmb.2009.03.004

22. Qiao H, He X, Schymura D, Ban L, Field L, Dani FR, et al. Cooperative interactions between odorant-binding proteins of Anopheles gambiae. Cell Mol Life Sci. 2011;68(10):1799-813. https://doi.org/10.1007/s00018-010-0539-8

23. Yin J, Choo YM, Duan H, Leal WS. Selectivity of odorant-binding proteins from the southern house mosquito tested against physiologically relevant ligands. Front Physiol. 2015;6:56. https://doi.org/10.3389/fphys.2015.00056

24. Jiang QY, Wang WX, Zhang Z, Zhang L. Binding specificity of locust odorant binding protein and its key binding site for initial recognition of alcohols. Insect Biochem Mol Biol. 2009;39(7):440-7. https://doi.org/10.1016/j.ibmb.2009.04.004

25. Plettner E, Lazar J, Prestwich EG, Prestwich GD. Discrimination of pheromone enantiomers by two pheromone binding proteins from the gypsy moth Lymantria dispar. Biochemistry. 2000;39(30):8953-62

26. Thireou T, Kythreoti G, Tsitsanou KE, Koussis K, Drakou CE, Kinnersley J, et al.

Identification of novel bioinspired synthetic mosquito repellents by combined ligand-based screening and OBP-structure-based molecular docking. Insect Biochem Mol Biol. 2018;98:48-61. https://doi.org/10.1016/j.ibmb.2018.05.001

27. Li F, Li D, Dewer Y, Qu C, Yang Z, Tian J, et al. Discrimination of Oviposition Deterrent Volatile beta-Ionone by Odorant-Binding Proteins 1 and 4 in the Whitefly Bemisia tabaci. Biomolecules. 2019;9(10). https://doi.org/10.3390/biom9100563
28. Yin J, Wang C, Fang C, Zhang S, Cao Y, Li K, et al. Functional characterization of odorant-binding proteins from the scarab beetle Holotrichia oblita based on semiochemical-induced expression alteration and gene silencing. Insect Biochemistry and Molecular Biology. 2019;104:11-9. https://doi.org/10.1016/j.ibmb.2018.11.002
29. Li L, Zhang WB, Shan YM, Zhang ZR, Pang BP. Functional Characterization of Olfactory Proteins Involved in Chemoreception of Galeruca daurica. Front Physiol. 2021;12:678698. https://doi.org/10.3389/fphys.2021.678698
30. Zhang XY, Zhu XQ, Gu SH, Zhou YL, Wang SY, Zhang YJ, et al. Silencing of odorant binding protein gene AlinOBP4 by RNAi induces declining electrophysiological responses of Adelphocoris lineolatus to six semiochemicals. Insect science. 2017;24(5):789-97. https://doi.org/10.1111/1744-7917.12365
31. Li J, Zhang L, Wang X. An Odorant-Binding Protein Involved In Perception Of Host Plant Odorants In Locust Locusta migratoria. Archives of insect biochemistry and physiology. 2016;91(4):221-9. https://doi.org/10.1002/arch.21319
32. Li R, Shan S, Song X, Khashaveh A, Wang S, Yin Z, et al. Plant volatile ligands for male-biased MmedOBP14 stimulate orientation behavior of the parasitoid wasp Microplitis mediator. International journal of biological macromolecules. 2022. https://doi.org/10.1016/j.ijbiomac.2022.11.149
33. Oliveira DS, Brito NF, Franco TA, Moreira MF, Leal WS, Melo ACA. Functional Characterization of Odorant Binding Protein 27 (RproOBP27) From Rhodnius prolixus

Antennae. Front Physiol. 2018;9:1175. https://doi.org/10.3389/fphys.2018.01175

34. Du Y, Chen J. The Odorant Binding Protein, SiOBP5, Mediates Alarm Pheromone Olfactory Recognition in the Red Imported Fire Ant, Solenopsis invicta. Biomolecules. 2021;11(11). https://doi.org/10.3390/biom11111595
35. Antony B, Johny J, Aldosari SA. Silencing the Odorant Binding Protein RferOBP1768 Reduces the Strong Preference of Palm Weevil for the Major Aggregation Pheromone Compound Ferrugineol. Front Physiol. 2018;9:252. https://doi.org/10.3389/fphys.2018.00252
36. Shorter JR, Dembeck LM, Everett LJ, Morozova TV, Arya GH, Turlapati L, et al. Obp56h Modulates Mating Behavior in Drosophila melanogaster. G3 (Bethesda, Md). 2016;6(10):3335-42. https://doi.org/10.1534/g3.116.034595
37. Ma S, Li LL, Yao WC, Yin MZ, Li JQ, Xu XW, et al. Two Odorant-Binding Proteins Involved in the Recognition of Sex Pheromones in Spodoptera litura Larvae. J Agric Food Chem. 2022;70(39):12372-82. https://doi.org/10.1021/acs.jafc.2c04335
38. Deng Y, Yan H, Gu J, Xu J, Wu K, Tu Z, et al. Molecular and functional characterization of odorant-binding protein genes in an invasive vector mosquito, Aedes albopictus. PLoS One. 2013;8(7):e68836. https://doi.org/10.1371/journal.pone.0068836
39. Diallo S, Shahbaaz M, Makwatta JO, Muema JM, Masiga D, Christofells A, et al. Antennal Enriched Odorant Binding Proteins Are Required for Odor Communication in Glossina f. fuscipes. Biomolecules. 2021;11(4). https://doi.org/10.3390/biom11040541
40. Pelletier J, Guidolin A, Syed Z, Cornel AJ, Leal WS. Knockdown of a mosquito odorant-binding protein involved in the sensitive detection of oviposition attractants. J Chem Ecol. 2010;36(3):245-8. https://doi.org/10.1007/s10886-010-9762-x
41. Biessmann H, Andronopoulou E, Biessmann MR, Douris V, Dimitratos SD, Eliopoulos E, et al. The Anopheles gambiae odorant binding protein 1 (AgamOBP1) mediates indole recognition in the antennae of female mosquitoes. PLoS One. 2010;5(3):e9471.

https://doi.org/10.1371/journal.pone.0009471

42. Manoharan M, Ng Fuk Chong M, Vaitinadapoule A, Frumence E, Sowdhamini R, Offmann B. Comparative genomics of odorant binding proteins in Anopheles gambiae, Aedes aegypti, and Culex quinquefasciatus. Genome Biol Evol. 2013;5(1):163-80. https://doi.org/10.1093/gbe/evs131
43. Biessmann H, Nguyen QK, Le D, Walter MF. Microarray-based survey of a subset of putative olfactory genes in the mosquito Anopheles gambiae. Insect Molecular Biology. 2005;14(6):575-89. https://doi.org/10.1111/j.1365-2583.2005.00590.x
44. Marinotti O, Calvo E, Nguyen QK, Dissanayake S, Ribeiro JMC, James AA. Genome-wide analysis of gene expression in adult Anopheles gambiae. Insect Molecular Biology. 2006;15(1):1-12.
45. Rund SS, Hou TY, Ward SM, Collins FH, Duffield GE. Genome-wide profiling of diel and circadian gene expression in the malaria vector Anopheles gambiae. Proc Natl Acad Sci USA. 2011;108(32):E421-30. https://doi.org/10.1073/pnas.1100584108.
46. Rund SS, Gentile JE, Duffield GE. Extensive circadian and light regulation of the transcriptome in the malaria mosquito Anopheles gambiae. BMC Genomics. 2013;14:218. https://doi.org/10.1186/1471-2164-14-218
47. Wu W, Li S, Yang M, Li Y, Zheng K, Akutse KS. Citronellal perception and transmission by Anopheles gambiae s.s. (Diptera: Culicidae) females. Sci Rep. 2020;10(1):18615. https://doi.org/10.1038/s41598-020-75782-3
48. Affonso RD, Guimaraes AP, Oliveira AA, Slana GBC, Franca TCC. Applications of Molecular Modeling in the Design of New Insect Repellents Targeting the Odorant Binding Protein of Anopheles gambiae. Journal of the Brazilian Chemical Society. 2013;24(3):473-82. https://doi.org/10.5935/0103-5053.20130059
49. Gaddaguti V, Venkateswara Rao T, Prasada Rao A. Potential mosquito repellent compounds of Ocimum species against 3N7H and 3Q8I of Anopheles gambiae. 3

Biotech. 2016;6(1):26. https://doi.org/10.1007/s13205-015-0346-x

50. Neto MFA, Santos C, Magalhaes-Junior JT, Leite FHA. Identification of novel Aedes aegypti odorant-binding protein 1 modulators by ligand and structure-based approaches and bioassays. J Biomol Struct Dyn. 2020:1-13. https://doi.org/10.1080/07391102.2020.1808074
51. Okoli BJ, Ladan Z, Mtunzi F, Hosea YC. Vitex negundo L. Essential Oil: Odorant Binding Protein Efficiency Using Molecular Docking Approach and Studies of the Mosquito Repellent. Insects. 2021;12(12). https://doi.org/10.3390/insects12121061
52. da Costa KS, Galucio JM, da Costa CHS, Santana AK, Dos Santos Carvalho V, do Nascimento LD, et al. Exploring the Potentiality of Natural Products from Essential Oils as Inhibitors of Odorant-Binding Proteins: A Structure- and Ligand-Based Virtual Screening Approach To Find Novel Mosquito Repellents. ACS Omega. 2019;4(27):22475-86. https://doi.org/10.1021/acsomega.9b03157
53. Kritsi E, Liggri PGV, Stamati ECV, Tsitsanou KE, Zographos SE, Michaelakis A, et al. A Combined Computational Methodology for the Discovery of Hit Compounds with Putative Insect Repellency Properties. ChemMedChem. 2022;17(16):e202200271. https://doi.org/10.1002/cmdc.202200271
54. Li TT, Liu WC, Zhu J, Yang YH, Ma C, Lu C, et al. Crystal structure and ligand identification of odorant binding protein 4 in the natural predator Chrysopa pallens. International journal of biological macromolecules. 2019;141:1004-12. https://doi.org/10.1016/j.ijbiomac.2019.09.043
55. Tsitsanou KE, Thireou T, Drakou CE, Koussis K, Keramioti MV, Leonidas DD, et al. Anopheles gambiae odorant binding protein crystal complex with the synthetic repellent DEET: implications for structure-based design of novel mosquito repellents. Cell Mol Life Sci. 2012;69(2):283-97. https://doi.org/10.1007/s00018-011-0745-z
56. Drakou CE, Tsitsanou KE, Potamitis C, Fessas D, Zervou M, Zographos SE. The crystal

structure of the AgamOBP1*Icaridin complex reveals alternative binding modes and stereo-selective repellent recognition. Cell Mol Life Sci. 2017;74(2):319-38. https://doi.org/10.1007/s00018-016-2335-6

57. Murphy EJ, Booth JC, Davrazou F, Port AM, Jones DN. Interactions of Anopheles gambiae odorant-binding proteins with a human-derived repellent: implications for the mode of action of n,n-diethyl-3-methylbenzamide (DEET). J Biol Chem. 2013;288(6):4475-85. https://doi.org/10.1074/jbc.M112.436386
58. Boix E. Eosinophil cationic protein. Methods Enzymol. 2001;341:287-305. https://doi.org/10.1016/s0076-6879(01)41159-.
59. Oldham NJ, Krieger J, Breer H, Svatos A. Detection and removal of an artefact fatty acid from the binding site of recombinant Bombyx mori pheromone-binding protein. Chemical Senses. 2001;26(5):529-31.
60. COLLABORATIVE COMPUTATIONAL PROJECT N. The CCP4 suite: programs for protein crystallography. Acta Crystallogr D Biol Crystallogr. 1994;50(Pt 5):760-3.
61. French S, Wilson K. Treatment of Negative Intensity Observations. Acta Crystallographica Section A. 1978;34(Jul):517-25.
62. Vagin A, Teplyakov A. MOLREP: an automated program for molecular replacement. Journal of Applied Crystallography. 1997;30:1022-5.
63. Murshudov GN, Vagin AA, Dodson EJ. Refinement of macromolecular structures by the maximum-likelihood method. Acta Crystallographica Section D-Biological Crystallography. 1997;53:240-55.
64. Schuttelkopf AW, van Aalten DM. PRODRG: a tool for high-throughput crystallography of protein-ligand complexes. Acta Crystallogr D Biol Crystallogr. 2004;60(Pt 8):1355-63. https://doi.org/10.1107/S0907444904011679
65. Chen VB, Arendall WB, 3rd, Headd JJ, Keedy DA, Immormino RM, Kapral GJ, et al. MolProbity: all-atom structure validation for macromolecular crystallography. Acta

Crystallogr D Biol Crystallogr. 2010;66(Pt 1):12-21. https://doi.org/10.1107/S0907444909042073

66. Joosten RP, Long F, Murshudov GN, Perrakis A. The PDB_REDO server for macromolecular structure model optimization. IUCrJ. 2014;1(Pt 4):213-20. https://doi.org/10.1107/S2052252514009324
67. Tian W, Chen C, Lei X, Zhao JL, Liang J. CASTp 3.0: computed atlas of surface topography of proteins. Nucleic Acids Research. 2018;46(W1):W363-W7. https://doi.org/10.1093/nar/gky473
68. Roberts E, Eargle J, Wright D, Luthey-Schulten Z. MultiSeq: unifying sequence and structure data for evolutionary analysis. Bmc Bioinformatics. 2006;7. https://doi.org/10.1186/1471-2105-7-382
69. Humphrey W, Dalke A, Schulten K. VMD: Visual molecular dynamics. Journal of Molecular Graphics & Modelling. 1996;14(1):33-8. https://doi.org/10.1016/0263-7855(96)00018-5
70. Laskowski RA, Swindells MB. LigPlot+: Multiple Ligand-Protein Interaction Diagrams for Drug Discovery. Journal of Chemical Information and Modeling. 2011;51(10):2778-86.
71. Robert X, Gouet P. Deciphering key features in protein structures with the new ENDscript server. Nucleic Acids Res. 2014;42(Web Server issue):W320-4. https://doi.org/10.1093/nar/gku316.
72. DeLano WL. The PyMOL Molecular Graphics System, DeLano Scientific. Palo Alto, CA, USA2002.
73. Campanacci V, Krieger J, Bette S, Sturgis JN, Lartigue A, Cambillau C, et al. Revisiting the specificity of Mamestra brassicae and Antheraea polyphemus pheromone-binding proteins with a fluorescence binding assay. J Biol Chem. 2001;276(23):20078-84. https://doi.org/10.1074/jbc.M100713200
74. Barone G, Del Vecchio P, Fessas D, Giancola C, Graziano G. Theseus: A new software

package for the handling and analysis of thermal denaturation data of biological macromolecules. Journal of thermal analysis. 1992;38(12):2779-90. https://doi.org/10.1007/BF01979752

75. Pelosi C, Saitta F, Wurm FR, Fessas D, Tine MR, Duce C. Thermodynamic stability of myoglobin-poly(ethylene glycol) bioconjugates: A calorimetric study. Thermochimica Acta. 2019;671:26-31. https://doi.org/10.1016/j.tca.2018.11.001
76. Pelosi C, Saitta F, Zerino C, Canil G, Biver T, Pratesi A, et al. Thermodynamic Evaluation of the Interactions between Anticancer Pt(II) Complexes and Model Proteins. Molecules. 2021;26(8). https://doi.org/10.3390/molecules26082376
77. Press WH, Flannery BP, Teukolsky SA, Vetterling WT. In Numerical recipes: The art of scientific computing (Press, C. U., ed.). pp. 521-538. Cambridge, UK. 1989.
78. Kröber T, Koussis K, Bourquina M, Tsitoura P, Konstantopoulou M, Awolola TS, et al. Odorant-binding protein-based identification of natural spatial repellents for the Africa malaria mosquito Anopheles gambiae. Insect Biochemistry and Molecular Biology. 2018;96:36-50.
79. Saitta F, Masuri J, Signorelli M, Bertini S, Bisio A, Fessas D. Thermodynamic insights on the effects of low-molecular-weight heparins on antithrombin III. Thermochimica Acta. 2022;713:179248. https://doi.org/10.1016/j.tca.2022.179248
80. Saitta F, Cannazza P, Donzella S, De Vitis V, Signorelli M, Romano D, et al. Calorimetric and thermodynamic analysis of an enantioselective carboxylesterase from Bacillus coagulans: Insights for an industrial scale-up. Thermochimica Acta. 2022;713:179247. https://doi.org/https://doi.org/10.1016/j.tca.2022.179247
81. D'Onofrio M, Ragona L, Fessas D, Signorelli M, Ugolini R, Pedò M, et al. NMR unfolding studies on a liver bile acid binding protein reveal a global two-state unfolding and localized singular behaviors. Archives of Biochemistry and Biophysics. 2009;481(1):21-9. https://doi.org/10.1016/j.abb.2008.10.017

82. Ausili A, Pennacchio A, Staiano M, Dattelbaum JD, Fessas D, Schiraldi A, et al. Amino acid transport in thermophiles: Characterization of an arginine-binding protein from Thermotoga maritima. 3. Conformational dynamics and stability. Journal of Photochemistry and Photobiology B: Biology. 2013;118:66-73. https://doi.org/https://doi.org/10.1016/j.jphotobiol.2012.11.004

83. Sleiman MH, Csonka R, Arbez-Gindre C, Heropoulos GA, Calogeropoulou T, Signorelli M, et al. Binding and stabilisation effects of glycodendritic compounds with peanut agglutinin. International journal of biological macromolecules. 2015;80:692-701. https://doi.org/10.1016/j.ijbiomac.2015.07.036

84. Davrazou F, Dong E, Murphy EJ, Johnson HT, Jones DN. New insights into the mechanism of odorant detection by the malaria-transmitting mosquito Anopheles gambiae. J Biol Chem. 2011;286(39):34175-83. https://doi.org/10.1074/jbc.M111.27[illegible]2

85. Y. Mao, X. Xu, W. Xu, Y. Ishida, W.S. Leal, J.B. Ames, J. Clardy, Crystal and solution structures of an odorant-binding protein from the southern house mosquito complexed with an oviposition pheromone, Proc Natl Acad Sci USA 107(44) (2010) 19102-7. https://doi.org/10.1073/pnas.1012274107